Akkermansia muciniphila identified as key strain to function in pathogen invasion and intestinal stem cell proliferation through Wnt signaling pathway

Xin Ma [a,b], Meng Li [a,b], Tingting Xu [b], Xinchen Zhou [a,b], Mengqi Qian [b], Zhiren Yang [a,b], Kai Cao [b], Xinyan Han [a,b,*]

[a] Hainan Institute of Zhejiang University, Yongyou Industry Park, Yazhou Bay Sci-Tech City, Sanya 572000, China

[b] Key Laboratory of Animal Nutrition and Feed Science in East China, Ministry of Agriculture, College of Animal Sciences, Zhejiang University, Hangzhou 310058, China

*Corresponding author

Xinyan Han

College of Animal Sciences, Zhejiang University, 866 Yuhangtang Road, Hangzhou 310058, China

E-mail: xyhan@zju.edu.cn

Credit author statement

XH and XM: Designed the experiments; XM and TX: Performed the experiments; XZ and MQ: Analyzed the data; XM and ML: Wrote the manuscript, which was edited by YZ, TX, MQ, XZ, KC and HX. All authors read and approved the final manuscript.

ABSTRACT

As the largest mucosal surface, the gut has built a physical, chemical, microbial and immune barrier to protect the body against pathogen invasion**.** The disturbance of gut microbiota aggravates pathogenic bacteria invasion and gut barrier injury. Fecal microbiota transplantation (FMT) is a promising treatment for microbiome-related disorders, where probiotic strain engraftment is a significant factor influencing FMT outcomes. The aim of this research was to explore the effect of FMT on antibiotic-induced microbiome-disordered (AIMD) model infected with enterotoxigenic *Escherichia coli* (ETEC). We used piglet, mouse and intestinal organoid models to explore the protective effects and mechanisms of FMT on ETEC infection. The results showed that FMT regulated gut microbiota and enhanced the protection of AIMD piglets against ETEC K88 challenge, as demonstrated by reduced intestinal pathogen colonization and alleviated gut barrier injury. *Akkermansia muciniphila* (*A. muciniphila*) and *Bacteroides fragilis* (*B. fragilis*) were identified as two strains that may play key roles in FMT. We further investigated the alleviatory effects of these two strains on ETEC infection in AIMD mice model, which revealed that *A. muciniphila* and *B. fragilis* relieved ETEC-induced intestinal inflammation by maintaining the proportion of Treg/Th17 cells and epithelial damage by moderately activating the Wnt/β-catenin signaling pathway, while the effect of *A. muciniphila* was better than *B. fragilis*. We therefore identified whether *A. muciniphila* protected against ETEC infection using basal-out and apical-out intestinal organoid models. *A. muciniphila* did protect the $Lgr5^+$ intestinal stem cells and stimulate proliferation and differentiation of intestinal epithelium, and the protective effects of *A. muciniphila* was reversed by Wnt inhibitor. FMT alleviated ETEC-induced gut barrier injury and intestinal inflammation in AIMD model. *A. muciniph*ila was identified as key strain in FMT to promote proliferation and differentiation of intestinal stem cells by mediating the Wnt/β-catenin signaling pathway.

Keywords: *Akkermansia muciniphila*; Wnt/β-catenin signaling pathway; Apical-out intestinal organoids; Gut barrier injury; Fecal microbiota transplantation.

Introduction

Growing evidences suggest that gut microbiota and its metabolites play important roles in modulating host health [1-3]. The most drastic exposure that leads to intestinal microbiota dysbiosis is antibiotic treatment, which kills commensal micro-organisms and inhibits these microbiota-mediated immune defense [4, 5]. The disturbance of intestinal microbiota may lead to disruptions of gut barrier and increase the susceptibility of host to pathogenic microbes [6, 7]. Several clinical studies have demonstrated that early-life exposure to antibiotic leads to gut microbiota dysbiosis that can impair host immune system maturation [8, 9]. Furthermore, the negative impact of antibiotics on gut microbiota in early life may even last for long periods throughout a lifetime, increasing the risk of gut diseases [10]. Enterotoxigenic *Escherichia coli* (ETEC) K88 infection is a common cause of diarrhea in humans and animals [11]. When ETEC adheres to intestinal epithelial cells, virulence factors interact with specific receptors to induce intestinal barrier injury and intestinal inflammatory responses [12]. Fecal microbiota transplantation (FMT) is a therapeutic intervention for reconstructing gut microbiota in gastrointestinal inflammatory diseases [13, 14]. Since FMT has been successful in treating Clostridium difficile infection and maintaining gut barrier, emerging investigation has been focused on other diseases [15-17]. Our previous study discovered that FMT alleviated early-life antibiotic-induced gut microbiota disorders and intestinal mucosa injury in neonatal piglet model [18]. However, whether FMT could remedy against ETEC K88 infection in antibiotic-induced gut microbiota-disordered (AIMD) piglets is still unknown. Simultaneously, the underlying mechanism of FMT and the gut microbes that confer its efficacy remain unclear.

Intestinal stem cell renewal is vital for the maintenance of gut barrier [19]. Mammalian intestinal epithelial cells are renewed approximately every 3-5 days with the migration of undifferentiated intestinal cells from the crypt to the top of the villi, accompanied by the differentiation of different types of epithelial cells [20]. The proliferation and differentiation of intestinal epithelium driven by intestinal stem cells, mainly crypt base columnar cells expressing R-Spondin receptor Lgr5, is a necessary process for repairing intestinal barrier

injury and preventing pathogens invasion [21, 22]. Sato et al. successfully cultured isolated intestinal stem cells into three-dimensional intestinal organoids with villous and crypt-like structural morphology for the first time [23]. Intestinal organoids contain various terminally differentiated cell types, including intestinal stem cell, tuft cell, absorptive cell, enteroendocrine cell, goblet cell, and Paneth cell, which have more advantages over single cell lines for *in vitro* study of intestinal regeneration [24]. Intestinal organoid is an ideal model for studying the interaction between intestinal epithelium and microorganisms in vitro, which can eliminate the complexity of animal models [25]. In traditional basal-out intestinal organoid models, the intestinal epithelium was in the interior of organoid spheroid, which restricted the interaction between intestinal epithelium and gut microbiota. Co et al. first established the intestinal organoid model with polarity reversal in human and mouse and evaluated the infection effects of the invasive pathogens with different polarity-specific patterns [26].

At present, high-throughput methods and bioinformatics platforms, such as genomics, transcriptomics and metabolomics, have been widely used to explore the relationship between host health and gut microbiota [27]. In the present study, we first investigated the effects of FMT on ETEC K88 infection in AIMD neonatal piglets, then by using bacterial 16S rDNA sequencing analysis, we identified *Akkermansia muciniphila* (*A. muciniphila*) as potential microbe to alleviate ETEC-induced intestinal barrier injury. We hypothesized that *A. muciniphila* could relieve intestinal barrier injury and intestinal inflammation by modulating the proliferation and differentiation of intestinal epithelium, and verified this hypothesis using *in vivo* mice experiments as well as *in vitro* porcine intestinal organoid models. Collectively, our results may provide theoretical basis that FMT is a promising mitigation method for pathogenic bacteria infection and a new strategy for the precise application of FMT in clinical and livestock production.

Materials and methods

Ethics statement

105 All animal experiments were performed according to the guidelines of the Animal Care
106 Committee of Zhejiang University School of Medicine (permit number SYXK 2012-0178).
107 The animal care protocol was approved by the Local Committee of Animal Use following the
108 Guide for the Care and Use of Laboratory Animals (NIH publication 86-23 revised 1985).
109

110 **Preparation of fecal microbiota suspension and bacterial strains**

111 The fecal microbiota suspension was prepared according to our previous method [18]. In
112 short, healthy adult Jinhua pigs that administrated medicinal feed additives or drugs for more
113 than 3 months were selected as fecal donors. The potential risks and infectious pathogens in
114 donor pigs were determined by serological and stool testing to ensure the safety of the porcine
115 FMT. Fresh fecal samples that collected from Jinhua pigs were transported in AnaeroPack
116 (Mitsubishi Gas Chemical, Japan) on ice to laboratory within 2 hours. The 50 g fecal samples
117 were homogenized in 250 mL sterile PBS, filtered through sterile stainless-steel strainer, and
118 then centrifuged at 4000 rpm for 10 min. The precipitate was resuspended in sterile PBS
119 solution containing 10% sterile glycerol, and the fecal microbiota suspension was stored at -
120 80°C. All the above preparation was performed in an anaerobic incubator (AW400SG
121 anaerobic workstations; Electrotek, UK). All the facilities and tools for the preparation of the
122 fecal microbiota suspension were sterilized prior to use. When processing the FMT, the fecal
123 microbiota suspension was thawed in 37°C water bath. ETEC K88 serotype O149:K91:K88ac
124 was purchased from the China Institute of Veterinary Drug Control (Beijing China), cultured
125 in Luria-Bertani medium (Qingdao Hope Bio-Technology Company, China), and incubated at
126 37°C in a shaker with 250 rpm overnight. *A. muciniphila* ATCC BAA-835 and *Bacteroides*
127 *fragilis* (*B. fragilis*) ATCC 25285 were purchased from Guangdong Microbial Culture
128 Collection Center (GDMCC, Guangzhou, China). *A. muciniphila* was cultured in brain heart
129 infusion media (OXOID, Thermo Fisher Biochemicals Ltd., UK) supplemented with 0.1%
130 mucin (Sigma-Aldrich, USA). *B. fragilis* was cultured in trypticase soy broth (Qingdao Hope
131 Bio-Technology Company, China) supplemented with 5% defibrinated sheep blood (Qingdao
132 Hope Bio-Technology Company, China). These two anaerobic bacteria strains were incubated

133 at 37°C in an anaerobic incubator with 10% H_2, 10% CO_2, and 80% N_2 (AW400SG anaerobic
134 workstations; Electrotek, UK). The cultures were centrifuged for 10 min at a speed of 4000
135 rpm, and the pellets were then resuspended in either aerobic or anaerobic PBS. Pasteurized *A.*
136 *muciniphila* and pasteurized *B. fragilis* were produced by pasteurization for 30 min at 70°C.
137
138 **Animals**
139 A total of 9 litters (9-11 piglets per litter) of Duroc × Landrace × Yorkshire ternary
140 hybrid neonatal piglets (aged 5 days) with identical birth dates and parities were obtained
141 from Anji Lvjiayuan Animal Husbandry Co. Ltd. (Zhejiang, China). Piglets were individually
142 housed in pens with appropriate environment of 24-26°C and 55-65% humidity. All newborn
143 piglets were fed with artificial milk substitutes, in which the nutrients reached the
144 requirements recommended by the National Research Council (NRC, 2012), and had *ad*
145 *libitum* access to water.
146 A total of 130 female C57BL/6 mice aged 5 weeks were obtained from Shanghai SLAC
147 Laboratory Animal, Co., Ltd. (SCXK (Zhejiang) 2017-0005; Shanghai, China). Mice were
148 housed in vinyl isolators in a room with 23 ± 1°C room temperature, 55-65% humidity and 12
149 h/12 h light/dark schedule. All mice had free access to water and food.
150 **Experimental design**
151 The piglets were randomly assigned to 3 groups (3 litters per group): the control group
152 (Con group), the ETEC K88 + PBS group (EP group) and the ETEC K88 + FMT group (EF
153 group). The piglets in EP and EF groups were orally inoculated with 2 ml ampicillin (120 mg
154 kg^{-1}) twice daily on day 1-3 of the experiment to disorder the intestinal resident microbiota,
155 then orally inoculated with ETEC K88 (1×10^9 CFU ml^{-1}) suspended in 2 ml sterile PBS
156 once daily on day 4-6 of the experiment. After ETEC K88 infection, the piglets in EF group
157 received 1.5 ml fecal microbiota suspension once daily by oral gavage for 6 days, while the
158 piglets in EP group received the same volume of sterile PBS. Meanwhile, the piglets in Con
159 group were orally inoculated with the same volume of sterile PBS throughout the experiment.
160 The doses of ampicillin and fecal microbiota suspension were based on a previous study by

161 Ma et al. [18]. The design of piglets' experiment is shown in Figure 1A. The weight of each
162 piglet was measured at both the beginning and the end of the experiment to calculate the ADG,
163 and diarrhea score (0, normal feces; 1, moist feces; 2, mild diarrhea; 3, severe diarrhea) was
164 recorded throughout the experiment. Six piglets (2 piglets per litter) were picked from each
165 group to be slaughtered at the end of the experiment (Day 13).

166 After acclimating for a week, mice were randomly assigned to 4 groups (n = 10 each):
167 the control group (C group), the ETEC K88 + PBS group (E group), the ETEC K88 + *A.*
168 *muciniphila* group (A group) and the ETEC K88 + *B. fragilis* group (B group). On day 1-3 of
169 the experiment, the mice in E, A and B groups were orally inoculated with 0.2 ml 15 mg ml^{-1}
170 ampicillin (Sigma-Aldrich, USA) twice daily to disorder the gut microbiota. On day 4-6 of the
171 experiment, the mice in E, A and B groups were infected with ETEC K88 (1×10^9 CFU)
172 suspended in 0.2 ml 0.1 M $NaHCO_3$ buffer (pH 9.0) by oral gavage once daily. Mice were
173 fasted for 12 h before infection. Meanwhile, the mice in C group were given the equal volume
174 of sterile PBS on day 1-6 of the experiment. On day 7-13 of the experiment, *A. muciniphila* (1
175 $\times 10^6$ CFU) and *B. fragilis* (1×10^8 CFU) suspended in 0.2 ml anaerobic sterile PBS were
176 administered intragastrically once daily to the mice in A group and B group respectively,
177 while mice in C and E groups received the same volume of anaerobic sterile PBS. The design
178 of mice's experiment is shown in Figure 1B. The concentrations of *A. muciniphila* and *B.*
179 *fragilis* were determined by examining the intestinal morphology and intestinal inflammatory
180 response of a 7 days-preliminary experiment that mice were randomized to 9 groups (n = 10
181 each) and orally administered 10^6 CFU live *A. muciniphila*, 10^8 CFU live *A. muciniphila*, 10^6
182 CFU pasteurized *A. muciniphila*, 10^8 CFU pasteurized *A. muciniphila*, 10^6 CFU live *B.*
183 *fragilis*, 10^8 CFU live *B. fragilis*, 10^6 CFU pasteurized *B. fragilis*, 10^8 CFU pasteurized *B.*
184 *fragilis* and same volume (0.2 ml) of anaerobic sterile PBS respectively (Figure S1). Mice
185 were orally infused with 0.2 ml 40 mg ml^{-1} 4 kDa fluorescein isothiocyanate-dextran (Sigma-
186 Aldrich, USA) 4 hours before sampling. At the end of the experiment (Day 14), six mice in
187 each group were randomly selected for ether anesthesia and neck dislocation.
188

189 **Culture and treatment of porcine intestinal organoid**

190 The cryovial of porcine intestinal organoid was kindly provided by Professor Li
191 Xiaoliang (Institute of Preventive Veterinary Medicine, College of Animal Sciences, Zhejiang
192 University, Hangzhou, China). The frozen organoids were thawed in a 37℃-water bath for 2
193 min, and then added 1 ml of DMEM/F-12 (Gibco, USA) with 1% bovine serum albumin
194 (BSA, BioFroxx, Germany) solution. The contents of the cryovial were mixed and transferred
195 to the 15 ml conical tube containing 2 ml of DMEM/F-12 with 1% BSA solution, and then
196 centrifuged at 200 × g for 5 min at 4℃. The organoids were resuspended in equal volume of
197 complete IntestiCult^{TM} Organoid Growth Medium (06010, StemCell^{TM} Technologies, Canada)
198 and Matrigel Matrix (356231, Corning, USA). The 50 μl of the 500-crypt suspension was
199 plated in the center of each well of the pre-warmed 24-well plate (3524, Corning, USA). The
200 plate was placed at 37℃ with 5% CO_2 for 10 min and then added 750 μl complete
201 IntestiCult^{TM} Organoid Growth Medium containing 100 μg ml^{-1} penicillin/streptomycin
202 (Invitrogen, USA) to each well. The culture medium was fully exchanged three times per
203 week. For the treatment, the frozen organoids were passaged two times after thawing.

204 For generation of apical-out organoids, the procedure of reversing the polarity of
205 organoids was performed according to a previously published protocol by Co et al [28].
206 Briefly, after growing in Matrigel Matrix with growth medium for 7 days, the Matrigel-
207 embedded organoids were gently dissolved with 500 μl cold 5 mM EDTA in D-PBS and
208 transferred to the 15 ml conical tube containing 10 ml of cold 5 mM EDTA. The tubes were
209 incubated on a rotating platform at 4℃ for 1 h, and then centrifuged at 200 × g for 3 min at
210 4℃. The organoids were resuspended in complete IntestiCult^{TM} Organoid Growth Medium
211 containing 100 μg ml^{-1} penicillin/streptomycin and transferred to ultra-low attachment 24-
212 well plate (3473, Corning, USA). The suspended organoids were cultured at 37℃ with 5%
213 CO_2 for 3 days.

214 To induce intestinal damage, the culture medium of basal-out and apical-out organoids
215 was changed to DMEM/F-12 containing ETEC K88 (10^6 CFU). After the invasion for 1 h, the
216 organoids were transferred to DMEM/F-12 containing 200 μg ml^{-1} penicillin/streptomycin for

217 1 h to kill residual extracellular bacteria. Then, the organoids were incubated in DMEM/F-12
218 containing *A. muciniphila* (10^5 CFU) for 1 h to detect the repair effect of *A. muciniphila*. In
219 addition, the organoids in WNT-C59 group were pretreated with the Wnt inhibitor Wnt-C59
220 (100 nM, AdooQ, China) for 24 h prior to damage. After co-cultivation, the organoids were
221 collected and resuspended in 4% paraformaldehyde (PFA, Servicebio, China) at 4℃ or
222 RNAiso Plus (Takara, Japan) at -80℃ for further analysis. For epithelial barrier integrity, the
223 apical-out organoids were resuspended in a solution of FD4 (2 mg ml^{-1}) diluted in DMEM/F-
224 12 without phenol red. The design of organoids' experiment is shown in Figure 1C.
225
226 **Real-time quantitative PCR (RT-qPCR) analysis**
227 Total RNA from intestinal tissue and organoids was extracted using TRIzol method
228 according to the precise instructions and cDNA was synthesized using PrimeScript™ RT
229 Master Mix (Takara, Japan). With cDNA as template, RT-qPCR was performed using TB
230 Green® *Premix Ex Taq*™ (Takara, Japan) on a LightCycler 480 System (Roche, Germany).
231 The real-time primers used in this study are listed in Table S1. The relative mRNA expression
232 of target genes was statistically analyzed based on the $2^{-\triangle\triangle Ct}$ method.
233
234 *Bacterial load and intestinal permeability analyses*
235 The bacterial load of ETEC K88 in piglets' jejunal and colonic mucosa was determined
236 by the absolute quantification. In brief, the gene of ETEC K88 was amplified by PCR (mK88-
237 F: GGAATGGAAAGTTGGTACAGGTCTT, mK88-R:
238 CCGGCATAAGATGCATTCACTTTC), and the PCR product was analyzed by agarose gel
239 electrophoresis. The specific band was excised and recovered, connected with pGM-T vector,
240 and transformed into high-efficiency chemoreceptor DH-5α cells. After culturing, the plasmid
241 DNA was extracted and sequenced. The RT-qPCR analysis was performed as the description
242 of section 2.5. The copy number of samples was calculated by the copy number of standard
243 and the standard curve.

244 For the detection of ETEC K88 load in mice, fresh feces, jejunum and colon tissue, liver,
245 spleen and kidney were homogenized in sterile normal saline using a tissue homogenizer
246 (Jingxin Industrial Development Co., Ltd., China), then the homogenates were diluted 10-fold
247 continuously, and the dilutions were plated on MacConkey Agar (Qingdao Hope Bio-
248 Technology Company, China). After incubating in aerobic incubator at 37℃ for 24 h, the
249 plates were counted three times. The results were presented as Lg CFU g^{-1} of samples.
250 For intestinal permeability assessment in mice, the serum fluorescence was detected
251 using a SpectraMax M5 plate reader (Molecular Devices, USA) at a 485 nm excitation
252 wavelength and a 535 nm emission wavelength. The standard curve was established from the
253 fluorescence of FD4 at concentrations of 0.005, 0.01, 0.02, 0.04, 0.08, 0.16 0.32, 0.64, 1.28,
254 2.56, 5.12 and 10.24 μg ml^{-1} to calculate the FD4 concentration.
255 For detection of epithelial barrier integrity in organoids, the apical-out organoids in the
256 FD4 solution were transferred to the slide and instantly imaged live by the laser scanning
257 confocal microscope IX81-FV1000 (Olympus, Japan) with FV10-ASW software (Olympus,
258 Japan).
259
260 **Histology and morphology analyses**
261 Jejunum and colon tissues were collected, fixed in 4% PFA or Carnoy's fluid and
262 embedded in paraffin. The tissue sections were stained with hematoxylin-eosin (H&E) or
263 periodic acid-Schiff (PAS) solution. The indexes related to the morphology of jejunum and
264 colon were measured by using Image Plus (v6.0). Scanning electron microscopy and
265 transmission electron microscopy (TEM) were performed according to the procedure of the
266 Bio-ultrastructure Analysis Lab of the Analysis Center of Agrobiology and Environmental
267 Sciences, Zhejiang University.
268
269 **Immunofluorescence analysis**
270 Jejunum tissues were fixed in 4% PFA, dehydrated, paraffin embedded and sectioned.
271 After antigen retrieval and blocking, the sections were incubated in primary antibodies at 4℃

272 overnight and secondary antibodies at room temperature for 50 min in the dark, followed by
273 staining with DAPI at room temperature for 10 min in the dark. The fixed organoids were
274 incubated in primary antibodies in blocking/permeabilization buffer at room temperature for 4
275 h, and then incubated in secondary antibodies together with DAPI and phalloidin (Servicebio,
276 China) in blocking/permeabilization buffer at room temperature for 2 h in the dark. The
277 fluorescence images were captured using a laser scanning confocal microscope IX81-FV1000
278 (Olympus, Japan) combined with FV10-ASW software (Olympus, Japan). The information of
279 primary and secondary antibodies is shown in Table S2.
280
281 **Western blot analysis**
282 Total protein was extracted by radioimmunoprecipitation assay lysis buffer and protein
283 concentration was determined by a BCA Assay Kit (Thermo Fisher Scientific, USA). Equal
284 protein amounts (60 μg) were electrophoresed on 10% sodium dodecyl sulphate-
285 polyacrylamide gel and the separated proteins were transferred onto the polyvinylidene
286 difluoride membranes (Millipore, USA) The membranes were blocked with Tris-buffered
287 saline with Tween (TBST) containing 5% BSA for 1 h at room temperature, and incubated
288 with the primary antibodies (Table S3) in TBST containing 3% BSA overnight at 4℃. After
289 several times washes in TBST, the membranes were incubated with secondary antibodies
290 (Table S3) in TBST containing 3% BSA for 1 h at room temperature. The protein bands were
291 visualized using SuperSignal® West Dura Extended Duration Substrate (Thermo Fisher
292 Scientific, USA), and quantified by Image J software.
293
294 **Microbiome sequencing analysis**
295 Total DNA was extracted from intestinal contents using the E.Z.N.A. ®Stool DNA Kit
296 (D4015, Omega, Inc., USA) according to the manufacturer's instructions. The quality of DNA
297 was detected by agarose gel electrophoresis, and total DNA was quantified by ultraviolet
298 spectrophotometer. Specific primers 341 F (5'-CCTACGGGNGGCWGCAG-3') and 805 R
299 (5'-GACTACHVGGGTATCTAATCC-3') were used for bacterial PCR amplification of 16S

300 rDNA V3-V4 hypervariable region. The PCR products were purified using AMPure XT beads
301 (Beckman Coulter Genomics, USA) and quantified by Qubit (Invitrogen, USA). The
302 amplicon pools were prepared for sequencing and the size and quantity of the amplicon
303 library were assessed on Agilent 2100 Bioanalyzer (Agilent, USA) and the Library
304 Quantification Kit for Illumina (Kapa Biosciences, USA), respectively. The libraries were
305 sequenced on NovaSeq PE250 platform. Samples were sequenced on an Illumina NovaSeq
306 platform according to the manufacturer's recommendations. Paired-end reads were assigned to
307 samples based on their unique barcode and truncated by cutting off the barcode and primer
308 sequence. Paired-end reads were merged using FLASH. Quality filtering on the raw reads
309 were performed under specific filtering conditions to obtain the high-quality clean tags
310 according to the fqtrim (v0.94). Chimeric sequences were filtered using Vsearch software
311 (v2.3.4). After dereplication using DADA2, the OTU were constructed by Amplicon
312 Sequence Variants to obtain the final feature table and feature sequence. Alpha diversity and
313 beta diversity were calculated by normalized to the same sequence randomly. Alpha diversity
314 is applied in analyzing complexity of species diversity for a sample through 4 indices,
315 including Chao1, Observed species, Shannon, Simpson, and all these indices in our samples
316 were calculated with QIIME2. Beta diversity was calculated by QIIME2, and the graphs were
317 drawn by R package. Blast was used for sequence alignment, and the feature sequences were
318 annotated with SILVA database for each representative sequence. Other diagrams were
319 implemented by using the R package (v3.5.2).
320
321 **Quantification of Short chain fatty acids**
322 The colonic contents (50 mg) were homogenized with 0.5 ml dH_2O in ball mill and then
323 centrifuged. The supernatant 1 (0.3 ml) was homogenized with 0.5 ml dH_2O and then
324 centrifuged. The supernatant 2 (0.5 ml) combined with supernatant 1 were mixed with 0.8 ml
325 of 2-Methylvaleric acid as internal standard solution and 0.1 ml 50% H_2SO_4. After
326 centrifuging, the supernatant was transferred into fresh glass vial for Gas chromatography-
327 mass spectrometry analysis, which was performed using an Agilent 7890B gas chromatograph

328 system coupled with an Agilent 5977B mass spectrometer. SCFAs were identified and
329 quantified by the retention time and standard curves of the standard solutions.

330 *Flow cytometry (FC) analysis*

331 Intestinal lamina propria cells were isolated by using Mouse Lamina Propria
332 Dissociation Kit (Miltenyi Biotec, Germany) according to the instruction. For cell surface
333 staining, the cells were incubated with FC block at 2-8℃ for 15 min, then were stained with
334 Live/Dead Dye at room temperature for 15 min, followed by washing with Stain Buffer. Cells
335 were incubated with specifical fluorescent antibodies (Table S4) at 2-8℃ for 30 min to label
336 immune cells. For intracellular factor staining, cells were fixed and permeabilized using
337 Transcription Factor Fix/Prem Buffer at 4℃ for 40 min, washed with 1 × Perm/Wash Buffer,
338 and stained with intracellular markers at 4℃ for 30 min. The stained cells were washed and
339 resuspended in PBS, and assessed by the 12-color FACSCelesta flow cytometer (Becton,
340 Dickinson and Company, USA). The data were analyzed using FlowJo software (v10.8.0).

341

342 **Isolation and culture of mouse intestinal crypts**

343 The jejunum proximal to the stomach was harvested immediately after mice were
344 sacrificed. After gently flushing with cold D-PBS (without calcium and magnesium) using
345 injection syringe, the intestinal segment was opened longitudinally and gently washed with
346 cold D-PBS three times. Then, the washed intestine was cut into 2 mm pieces with scissors,
347 which fell into a 50 ml conical tube containing 15 ml cold D-PBS. The rinsing procedure that
348 using the 10 ml serological pipette to gently pipette the intestinal pieces up and down three
349 times and then aspirate off the supernatant and add 15 ml fresh cold D-PBS was repeated 10-
350 15 times until the supernatant was clear. The intestinal pieces were resuspended in 25 ml
351 Gentle Cell Dissociation Reagent (GCDR, StemCell^{TM} Technologies, Canada) and incubated
352 at room temperature for 15 min on a rocking platform. After incubation, the intestinal pieces
353 were resuspended in 10 ml cold D-PBS containing 0.1% BSA, supernatant was filtered
354 through a 70 μm filter (Corning, USA), and filtrate was collected and labeled as fraction 1.
355 Repeat the above step three times to obtain fractions 2-4. The fractions were centrifuged at

356 290 × g for 5 min at 4°C and resuspended in 10 ml cold DMEM/F-12 with 15 mM HEPES.
357 The quality of the fractions was assessed by using an inverted microscope. The fraction which
358 enriched for intestinal crypts was selected, centrifuged and resuspended in equal volume of
359 complete IntestiCult™ Organoid Growth Medium (06005, StemCell™ Technologies, Canada)
360 and Matrigel Matrix. The 50 μl of the 500-crypt suspension was plated in the center of each
361 well of the pre-warmed 24-well plate. The plate was placed at 37°C with 5% CO_2 for 10 min
362 and then added 750 μl complete IntestiCult™ Organoid Growth Medium containing 100 μg
363 ml^{-1} penicillin/streptomycin to each well. The culture medium was fully exchanged three
364 times per week. After 7 to 10 days of culture, the organoids were passaged using 1:6 split ratio.
365 The images of organoids were captured using inverted microscope (Nikon, Japan). The
366 surface areas of organoids were measured using ImageJ software (v1.8.0). The forming
367 efficiency (%) = (number of mature organoids growing after 5 days / number of crypts seeded)
368 × 100%.
369

370 **Statistical analysis**

371 Data were statistically analyzed by SPSS (v26.0) software, and all data are presented as
372 means ± standard deviation (SD). P value < 0.05 was considered significant. Kolmogorov-
373 Smirnov test was used to determine whether the data followed the normal distribution.
374 Comparisons between two groups were executed by unpaired Student's *t*-test or Mann-
375 Whitney *U*-test, and comparisons among three groups were executed by one-way ANOVA or
376 Kruskal-Wallis followed by Dunn's multiple comparisons.
377

378 **Results**

379 **FMT enhanced the protection of AIMD piglets against ETEC K88 challenge**

380 ETEC K88 infection is a leading cause of diarrhea in humans and animals. We set out to
381 explore whether FMT protected against ETEC K88 challenge. As shown in Figure S2A and B,
382 decreased average daily gain (ADG) and increased diarrhea score were observed in AIMD
383 piglets at day 3 and day 6 after ETEC K88 infection, and these symptoms were relieved by

384 FMT treatment. We next detected the pathogen colonization in mucosal tissues and found that
385 FMT significantly decreased the copies of ETEC K88 in the jejunal and colonic mucosa
386 (Figure S2C). To address whether FMT could protect intestinal barrier against ETEC K88
387 infection, intestinal barrier integrity and inflammatory cytokine levels were detected. FMT
388 decreased the expression of proinflammatory cytokines (*TNF-α*, *IL-1β* and *IL-6*) and
389 increased levels of anti-inflammatory cytokines (*IL-10* and *TGF-β1*) in the jejunum ($P < 0.01$,
390 Figure S2D). Jejunal scanning electron microscopy showed that the villi (Figure 2A top) in
391 ETEC K88 group (EP group) were short and coarse, and there existed obvious rod-shaped
392 bacterial adhesion on the surface of microvilli (Figure 2A bottom), while FMT reversed villi
393 and microvilli injury caused by ETEC K88. In addition, the reduced mRNA and protein levels
394 of the tight junctions (ZO-1, claudin and occludin) and adheren junctions (β-catenin and E-
395 cadherin) caused by ETEC K88 challenge were also reversed by FMT treatment in the
396 jejunum (Figure 2B-C). We then evaluated the expression of Mucin 2 (MUC2) in the jejunum
397 using immunofluorescence staining. As shown in Figure 2D, ETEC K88 infection reduced the
398 expression of MUC2, which was significantly increased following FMT administration. These
399 results indicated that FMT enhanced the protection of AIMD piglets against ETEC K88
400 challenge.
401
402 ***A. muciniphila* and *B. fragilis* were identified as two key strains in FMT**
403 Our previous study showed that FMT enhanced intestinal barrier by modulating gut
404 microbiota and related metabolites [29]. We assessed the variation of gut microbiota (Figure
405 S3A-D) and short chain fatty acids (SCFA) metabolites in ETEC K88-challenged piglets. The
406 principal coordinate analysis (PCoA) and non-metric multidimensional scaling (NMDS)
407 showed that gut microbiota between two groups clustered separately (Figure S3C and S3D).
408 The Anosim analysis ($R = 0.396$, $P = 0.02$) and UPGMA clustering analysis also indicated
409 that FMT altered the structure of the gut microbiota in ETEC K88-challenged piglets (Figure
410 3A and 3B). Linear discriminant analysis (LDA) effect size (LEfSe) analysis verified that *B.*
411 *fragilis* and *Akkermansia* were changed significantly with an upper 4 LDA score after FMT

412 administration (Figure 3C). *Akkermansia* was not annotated to the species level, which might
413 due to the Mother annotation method applying the Least Common Ancestor algorithm. When
414 two different annotation results of the same classification level were obtained, the default
415 common taxon of the upper level was the last annotation result. Therefore, we compared the
416 Operational Taxonomic Units (OUT) sequence of *Akkermansia* in the National Center for
417 Biotechnology Information database by using Blast method based on Best Hit algorithm, and
418 the result was *A. muciniphila*. Furthermore, FMT significantly increased the production of
419 SCFA metabolites, including acetic acid, propionic acid, butyric acid, isobutyric acid,
420 isovaleric acid and hexanoic acid (Figure 3D). These results demonstrated that FMT regulated
421 gut microbiota and SCFA metabolites in ETEC K88-challenged piglets. *A. muciniphila* and B.
422 fragilis were identified as two strains that may play key roles in FMT.
423

424 ***A. muciniphila* and *B. fragilis* maintain intestinal barrier function of ETEC-induced**
425 **mice**

426 We further investigated whether these two strains exerted protective effects on ETEC
427 infection in AIMD mice model. As shown in Figure 4A, ETEC K88 infection led to intestinal
428 morphology damage, which was relieved by *A. muciniphila* and *B. fragilis* treatment.
429 Correspondingly, scanning electron microscopy showed that *A. muciniphila* and *B. fragilis*
430 increased the height and number of microvilli and ameliorated the distribution of intercellular
431 junction in the jejunum and colon (Figure 4B). In addition, *A. muciniphila* and *B. fragilis*
432 treated mice showed thicker mucus layer and increased numbers of goblet cells than ETEC
433 K88-infected mice (Figure 4C). Due to the fact that *A. muciniphila* and *B. fragilis* improved
434 mucus secretion, the expression of MUC2 secreted by goblet cells was determined in the
435 jejunum and colon. As expected, the relative mRNA and protein expressions of MUC2 were
436 significantly increased in the jejunum of *A. muciniphila* and *B. fragilis* treated mice (Figure
437 4D). However, only *A. muciniphila* could upregulated MUC2 protein expression in the colon
438 of treated mice (Figure 4D). Furthermore, we investigated the diffusion of ETEC K88 in feces
439 and organs after infection. ETEC K88 infection surged the number of *Escherichia coli* in the

440 feces, jejunum, colon, liver, spleen and kidney (Figure S4A). *A. muciniphila* and *B. fragilis*
441 treatment dramatically decreased the amount of ETEC K88 in these tissues (Figure S4A),
442 indicating a reduced translocation of ETEC K88 in the tissues and organs. The concentration
443 of 4 kDa fluorescein isothiocyanate-dextran (FD4) in the serum has been commonly used as
444 an indicator of intestinal permeability. As shown in Figure S4B, *A. muciniphila* and *B. fragilis*
445 significantly decreased serum FD4 concentration, indicating *A. muciniphila* and *B. fragilis*
446 enhanced intestinal barrier integrity.

447 ETEC K88 adheres to intestinal epithelial cells and induces gut inflammation [30]. As
448 demonstrated in Figure 5A, ETEC K88 decreased the relative mRNA expression of anti-
449 inflammatory cytokines *IL-10* and *TGF-β* was decreased and increased levels of pro-
450 inflammatory cytokines *TNF-α*, *IL-1β*, *IL-6* and *IFN-γ*, which was reversed in A and B group,
451 indicating that *A. muciniphila* and *B. fragilis* ameliorated ETEC K88-induced intestinal
452 inflammation. Intestinal inflammatory response is closely related to immune cells. Treg cells
453 secrete anti-inflammatory cytokines IL-10 and TGF-β to alleviate intestinal inflammation.
454 Conversely, Th17 cells produce pro-inflammatory cytokines, such as IFN-γ and IL-17, which
455 aggravate intestinal inflammation. The dynamic balance of Treg and Th17 cells plays an
456 important role in intestinal immunity. Therefore, we used flow cytometry to analyze the
457 proportion of the immune cells isolated from jejunal lamina propria in the innate and adaptive
458 immune system. Treg cells were labeled with $CD25^{+}Foxp3^{+}$ cells, Th17 cells were labeled
459 with $CD4^{+}ROR\gamma t^{+}$ cells, and mature dendritic cells were labeled with $CD86^{+}CD11C^{+}$ cells.
460 ETEC K88 infection significantly decreased the proportion of Treg cells and mature dendritic
461 cells and increased the proportion of Th17 cells, while oral administration of *A. muciniphila*
462 or *B. fragilis* significantly reduced the proportion of Th17 cells and increased the proportion
463 of mature dendritic cells (Figure 5B). Moreover, compared with ETEC K88 group (E group),
464 the proportion of Treg cells in ETEC K88 + *A. muciniphila* group (A group) was significantly
465 increased ($P < 0.01$), and the proportion of Treg cells in the ETEC K88 + *B. fragilis* mouse
466 group (B group) had an increasing trend ($P = 0.59$), indicating FMT maintained the
467 proportion of Treg/Th17 cells in ETEC K88-infected mice.

468

469 ***A. muciniphila* accelerated intestinal epithelial proliferation**

470 Since oral administration of *A. muciniphila* and *B. fragilis* mitigated intestinal mucosal
471 injury, we set out to explore their effects on the proliferation and differentiation of intestinal
472 epithelium. ETEC K88 infection prominently decreased *Ki67* and *Lyz* expression and the
473 number of $Ki67^+$ cells and Lyz^+ Paneth cells in the crypt of the jejunum (Figure 6A and 6B). *A.*
474 *muciniphila* and *B. fragilis* increased *Ki67* and *Lyz* expression and the number of $Ki67^+$ cells.
475 However, only *A. muciniphila* enhanced the number of Lyz^+ Paneth cells, suggesting that *A.*
476 *muciniphila* accelerated the proliferation and differentiation of intestinal epithelial cells. Lgr5-
477 labeled active intestinal stem cells are the driving force of intestinal epithelial proliferation
478 and differentiation after intestinal injury. ETEC K88 infection significantly increased the
479 relative mRNA expression of *Lgr5*, *Wnt3*, *Axin2*, *Ctnnb1* in jejunum mucosa and had no
480 significant impact on *Notch1* and *Hes1* expression (Figure 6C). *A. muciniphila* and *B. fragilis*
481 inhibited the upregulation of *Lgr5*, *Wnt3*, *Axin2* and *Ctnnb1* at transcriptional level caused by
482 ETEC K88 infection and had no significant effect on *Notch1* and *Hes1* levels. Western blot
483 analysis also showed that *A. muciniphila* and *B. fragilis* inhibited the upregulation Lgr5, Wnt3,
484 Active β-catenin, C-Myc and CyclinD1 at protein level, and the effect of *A. muciniphila* was
485 better than that of *B. fragilis* (Figure 6D). These results implied that *A. muciniphila* regulated
486 the expression of $Lgr5^+$ intestinal stem cells in ETEC K88-challenged mice and regulated
487 Wnt/β-catenin signaling pathway rather than Notch signaling pathway.

488 We next isolated jejunal crypt from mice and explore whether *A. muciniphila* or *B.*
489 *fragilis* influenced the ability of intestinal stem cells growing into intestinal organoids in vitro.
490 In ETEC K88-infected piglets, the crypts formed into undifferentiated spherical organoids,
491 while in *A. muciniphila* or *B. fragilis* treated piglets, the crypts generated mature organoids
492 with bud structure (Figure 7A). We statistically analyzed the surface area and forming
493 efficiency of the intestinal organoids. As shown in Figure 7B, the organoids derived from
494 ETEC K88-infected mice had smaller surface area and lower forming efficiency than those
495 from control mice. *A. muciniphila* treatment led to larger surface area and higher forming

496 efficiency of the intestinal organoids. The surface area of intestinal organoids in *B. fragilis*
497 group was larger than that in ETEC group, while there was no significant difference in
498 forming efficiency between two groups. Meanwhile, the relative mRNA expression of genes
499 related to the proliferation and differentiation at the intestinal organoid level was consistent
500 with the results of jejunal mucosa *in vivo* (Figure 8C). These results suggested that *A.*
501 *muciniphila* accelerated intestinal epithelial proliferation and regulated Wnt/β-catenin
502 signaling pathway in vitro.
503
504 ***A. muciniphila* protected intestinal organoids against ETEC infection via Wnt signaling**
505 We further used basal-out and apical-out intestinal organoid models to explore the effects
506 and mechanisms of *A. muciniphila* on ETEC K88 infection. The relative mRNA expression of
507 *villin*, *ZO-1*, *Ki67*, *Lyz*, *MUC2*, *Lgr5*, *Wnt3a, β-catenin* and the fluorescence intensity of villin,
508 Ki67, Lgr5, Wnt3a and β-catenin in basal-out intestinal organoids were significantly down-
509 regulated upon ETEC exposure (Figure 8A-G). *A. muciniphila* upregulated Lgr5, Wnt3a and
510 *β-catenin* expression in ETEC-infected organoids, while these effects were inhibited by Wnt-
511 C59 treatment (Figure 8A-G). The results suggested that *A. muciniphila* increased the number
512 of $Lgr5^{+}$ intestinal stem cells and activated Wnt signaling, but not promoted the proliferation
513 and differentiation of basal-out gut organoids. In basal-out intestinal organoid models, the
514 intestinal epithelium was in the interior of organoid spheroid, which restricted the interaction
515 between intestinal epithelium and *A. muciniphila*. Therefore, we reversed the polarity of
516 basal-out intestinal organoids by removing the Matrigel from the culture system and
517 suspending intestinal organoids in the culture (Figure S5A). In basal-out intestinal organoids,
518 the apical surface was outward to make it accessible to *A. muciniphila*. Under confocal
519 microscopy, the F-actin of basal-out intestinal organoid was located in the inside of the
520 spheroids, while the F-actin of the apical-out intestinal organoid was outside the spheroids,
521 indicating that the polar reversal intestinal organoid model was successfully constructed
522 (Figure S5B). We conducted FD4 permeation test in apical-out intestinal organoid model, and
523 co-cultivation with *A. muciniphila* restored the epithelial barrier integrity of organoids

524 challenged by ETEC K88 (Figure 9A, H). *A. muciniphila* not only increased the mRNA
525 expression of *ZO-1*, *Lyz* and *MUC2* in the ETEC K88 infected apical-out intestinal organoids,
526 but also up-regulated the protein expression of villin, Wnt3a, β-catenin and the number of
527 $Lgr5^+$ and $Ki67^+$ cells (Figure 9B-G, I). Moreover, *A. muciniphila* also relieved the
528 inflammatory response of the ETEC K88 infected apical-out intestinal organoids, as
529 determined by decreasing proinflammatory cytokines, inducing *TNF-α*, *IL-1β*, *IL-6* and *IFN-γ*,
530 and increasing anti-inflammatory cytokines *IL-10* and *TGF-β* (Figure 9J). However, the
531 moderating effect of *A. muciniphila* on the apical-out intestinal organoids disappeared after
532 Wnt-C59 exposure. Taken together, *A. muciniphila* accelerated the proliferation and
533 differentiation of the intestinal stem cells and ameliorated the intestinal barrier injury and
534 inflammation induced by ETEC K88. *A. muciniphila* protected intestinal organoids against
535 ETEC infection via Wnt signaling.
536
537 **Discussion**
538 The homeostasis of gut microbiota is a major contributor to host health. Intestinal
539 dysbiosis increases intestinal colonization of antibiotic-resistant and pathogenic bacteria.
540 Antibiotic treatment is the most drastic exposure leading to gut dysbiosis and pathogen
541 invasion [5]. Early-life exposure to antibiotic leads to gut microbiota dysbiosis and impair
542 host immune system maturation, which may even last for long periods throughout life [8, 9].
543 Researchers have made a lot of attempts to prevent or inhibit antibiotic-induced dysbiosis.
544 Our previous study showed that FMT alleviates early-life antibiotic-induced gut microbiota
545 dysbiosis and mucosa injuries in a neonatal piglet model [31]. Our study aimed to investigate
546 whether FMT increases early-life antibiotic induced neonatal piglet against pathogen invasion.
547 ETEC K88 is one of the most common pathogens in humans and animals and causes
548 intestinal inflammation and diarrhea symptoms [32]. Studies demonstrated that ETEC K88
549 infection led to pro-inflammatory cytokine upregulation and intestinal mucosal barrier injury
550 [33, 34]. In ETEC-induced neonatal piglets, ZO-1 and Claudin-2 levels in ileum of were
551 significantly decreased after ETEC K88 infection [33]. In accordance with the above results,

552 the present study showed that ETEC K88 infection increased the expression of pro-
553 inflammatory cytokines and reduced the expression of intercellular junction proteins in AIMD
554 piglets. Since FMT has been successful in treating Clostridium difficile infection and
555 maintaining gut barrier, emerging investigation has been focused on other diseases [15, 16].
556 Our previous study discovered that FMT ameliorated gut microbiota disorder and intestinal
557 barrier injury induced by antibiotics [18]. Geng et al. demonstrated that FMT diminished the
558 inflammatory response and the destruction of epithelial integrity in piglets challenged with
559 lipopolysaccharide [35]. In the present study, we found that FMT dampened ETEC K88-
560 induced pro-inflammatory cytokines upregulation and improved the intestinal morphology. In
561 addition, the number of ETEC K88 in jejunal and colonic mucosa was significantly decreased
562 following FMT, which was consistent with the observation of jejunal microvilli under SEM,
563 showing the absence of rod-shaped bacterial adhesion in the EF group. ETEC infection was
564 reported to reduce the MUC2 expression by destroying goblet cells or directly degrading
565 MUC2, thereby damaging the integrity of the intestinal epithelial barrier [36]. Our results
566 demonstrated that FMT enhanced the expression of MUC2 and increased the expression of
567 ZO-1, claudin, occludin, β-catenin and E-cadherin at mRNA and protein levels, indicating that
568 FMT improved the intercellular junctions between intestinal epithelial cells and restored the
569 integrity of the intestinal mucosal barrier to reduce the colonization and invasion of ETEC
570 K88.

571 Intestinal microbiota plays a key role in maintaining gut mucosal barrier and resistance
572 to pathogen invasion [37-40]. Antibiotic-induced gut microbiota-disorders have been reported
573 to disrupt gut barrier and increase the susceptibility of host to pathogenic microbes [41]. Our
574 previous study showed that FMT enhanced intestinal barrier by modulating gut microbiota
575 and SCFAs [29]. So, we further probed the changes of gut microbiota in AIMD piglets
576 infected with ETEC K88. The results showed that FMT regulated gut microbiota and SCFAs
577 metabolism in ETEC K88-challenged piglets. LEfSe analysis manifested that *B. fragilis* and *A.*
578 *muciniphila* were the key differential bacteria between three groups. *A. muciniphila* utilizes
579 mucin as the only carbon and nitrogen source for its growth in the gut, and its metabolite

580 SCFAs can facilitate MUC2 secretion by goblet cells to maintain the dynamic balance of
581 intestinal mucus layer [42]. *A. muciniphila* negatively correlated with many diseases,
582 including diabetes, obesity and inflammatory bowel diseases [43-45]. It has been reported that
583 *A. muciniphila* effectively inhibited intestinal inflammatory response and elevated epithelial
584 barrier function [46-48]. Meanwhile, *B. fragilis* could decompose mucin by lipid-anchored
585 enzymes and interact with intestinal epithelial cells, thereby altering intestinal permeability
586 and repairing intestinal epithelial barrier [49, 50]. Deng et al. reported that *B. fragilis* altered
587 macrophage phenotype and increased the phagocytosis of macrophages to restrain pathogens
588 colonization [51]. Hence, we speculated that FMT increased the relative abundance of *A.*
589 *muciniphila* and *B. fragilis* in the intestine and alleviate intestinal barrier injury and intestinal
590 inflammation caused by ETEC K88 infection.

591 Since *A. muciniphila* and *B. fragilis* were identified as two strains that may play key
592 roles in FMT, we further investigate whether *A. muciniphila* and *B. fragilis* exerted protective
593 effect on ETEC K88 infection in AIMD mice model. We found that *A. muciniphila* and *B.*
594 *fragilis* maintained normal gut morphology after ETEC K88 infection, repaired the integrity
595 of intestinal mucosal barrier as evidenced by the reduced FD4 concentration in serum,
596 colonized in the intestine and inhibit the translocation of ETEC K88, and reduced the
597 intestinal inflammation, which may have been attributed to the increased proportion of Treg
598 cells and mature dendritic cells and the decreased proportion of Th17 cells. These results are
599 consistent with the protective role of *A. muciniphila* and *B. fragilis* in dextran sulphate sodium
600 salt induced enteritis model [52-54]. Intestinal stem cell renewal is vital to maintaining the gut
601 barrier [19]. Ki67 is widely expressed in proliferating cells and presents a reliable indicator of
602 cell proliferation activity [55]. Ki67 reaches its peak during the division stage with short half-
603 life period and easy degradation [55]. In our study, *A. muciniphila* and *B. fragilis* increased
604 the number of $Ki67^{+}$ cells and the mRNA expression of *Lyz*, suggesting that *A. muciniphila*
605 and *B. fragilis* accelerated the proliferation and differentiation of intestinal epithelium. Paneth
606 cells not only produce antimicrobial peptides and express key niche signals that regulate stem
607 cells, but also secrete activators that dynamically modulate Wnt/β-catenin signaling pathway

608 [56]. The Wnt/β-catenin signaling pathway is essential for the proliferation and differentiation
609 of intestinal stem cells [57]. When the Wnt receptors are activated, the multiprotein
610 degradation complex is rapidly inhibited, which allows β-catenin to accumulate and
611 subsequently migrate to the nucleus and binds to the transcription factors of T cell factor
612 family and lymphoid enhancer-binding factor family to drive the expression of genes that
613 regulate the stem cells, including Lgr5, c-Myc and Cyclin D1 [58]. The c-Myc and Cyclin D1
614 are cyclins that positively regulate cell cycle from the G1 phase to S phase, thus inducing cell
615 cycle progression and promote cell proliferation [59]. In the present study, *A. muciniphila*
616 moderately activated Wnt/β-catenin signaling pathway and maintain the suitable expression of
617 Wnt, Active-β-catenin, Lgr5, c-Myc and Cyclin D1. Simultaneously, *B. fragilis* also avoid the
618 overactivation of the Wnt/β-catenin signaling pathway caused by the ETEC K88 infection,
619 while the impact of *B. fragilis* was not as obvious as *A. muciniphila*. Consistent with the *in*
620 *vivo* results, *A. muciniphila* repaired the damaged intestinal epithelium caused by the ETEC
621 K88 infection by modulating the Wnt/β-catenin signaling pathway.

622 Intestinal organoid is an ideal model for studying the interaction between intestinal
623 epithelium and microorganisms in vitro, which can eliminate the complexity of animal models
624 and avoid the unicity of the traditional intestinal epithelial cells [25]. In order to further verify
625 whether *A. muciniphila* attenuated ETEC K88 infection through Wnt/β-catenin signaling
626 pathway, basal-out and apical-out porcine intestinal organoid models was used. Notably, we
627 found that the ETEC K88 infection down-regulated Wnt/β-catenin signaling pathway *in vitro*,
628 which was inconsistent with the results *in vivo*. A recent study showed that the addition of 400
629 ng ml^{-1} STp, an enterotoxin of ETEC, could suppress Wnt/β-catenin signaling pathway of
630 porcine intestinal organoids [60]. It is speculated that the reason for the difference results
631 might be related to the difference in the processing time of the *in vivo* and *in vitro* treatment.
632 In spite of the slight stimulation of *A. muciniphila* on the proliferation and differentiation of
633 infected intestinal organoids, *A. muciniphila* up-regulated the Wnt/β-catenin signaling
634 pathway and had protective effects on $Lgr5^{+}$ intestinal stem cells. In basal-out intestinal
635 organoid models, the intestinal epithelium was in the interior of organoid spheroid, which

636 restricted the interaction between intestinal epithelium and *A. muciniphila*. Co et al. first
637 established the intestinal organoid model with polarity reversal in human and mouse and
638 evaluated the infection effects of the invasive pathogens with different polarity-specific
639 patterns [26], *Salmonella enterica serovar Typhimurium* and *Listeria monocytogenes*, on
640 polarity reversal intestinal organoids. Subsequently, Li et al. first applied the porcine intestinal
641 organoids with polarity reversal to investigate the infectivity and antiviral immune responses
642 of porcine transmissible gastroenteritis virus [61]. In addition, studies on host-pathogen
643 interactions using polarity reversal intestinal organoids have also been reported in the sheep
644 and chickens [62, 63]. But up to now, there are few reports on the interaction between host
645 and symbiotic microorganism using polarity reversal intestinal organoids. Here, we utilized
646 porcine polarity reversal intestinal organoids to make *A. muciniphila* directly interacting with
647 the intestinal epithelium. Our results showed that *A. muciniphila* alleviated the injury of
648 polarity reversal intestinal organoids induced by ETEC K88. In agreement with the *in vivo*
649 results, *A. muciniphila* restrain the intestinal inflammation caused by the ETEC K88 infection
650 in polarity reversal intestinal organoids. Additionally, the alleviatory effect of *A. muciniphila*
651 on ETEC K88 infection via the Wnt/β-catenin signaling pathway was confirmed with the
652 addition of Wnt inhibitor Wnt-C59. The promoted proliferation and differentiation in the
653 basal-out and apical-out intestinal organoids after co-culturing with *A. muciniphila* were
654 reversed with Wnt-C59.

655 In conclusion, we found that FMT relieved intestinal inflammation and improved
656 intestinal barrier function in AIMD piglets infected with ETEC K88. *A. muciniphila* was
657 identified as key strain in FMT to promote the proliferation and differentiation of $Lgr5^+$
658 intestinal stem cells by mediating the Wnt/β catenin signaling pathway. The study revealed the
659 possible mechanism that FMT alleviates the intestinal barrier injury.

660

661 **DECLARATIONS**

662 **Ethics approval and Consent to participate**

All animal experiments were performed according to the guidelines of the Animal Care Committee of Zhejiang University School of Medicine (permit number SYXK 2012-0178). The animal care protocol was approved by the Local Committee of Animal Use following the Guide for the Care and Use of Laboratory Animals (NIH publication 86-23 revised 1985).

Consent for publication

Not applicable.

Availability of data and material

The raw sequences derived from microbiome analysis for this study can be found in the Sequence Read Archive (SRA) (https://www.ncbi.nlm.nih.gov/sra/PRJNA837047). And all datasets analyzed in the present study are available from the corresponding author on reasonable request.

Competing interests

The authors declared that the work was carried out in the absence of any commercial or financial relationships that could be construed as a potential conflict of interest.

Funding

This research was supported by the National Natural Science Foundation of China (grant number 32172765).

Acknowledgments

We appreciated the Experimental Teaching Center, College of Animal Science, Zhejiang University for providing the AW400SG anaerobic workstations.

References

1. Ee C, Rcr M, K V, Ee B. Gut microbial metabolites in obesity, NAFLD and T2DM. Nature reviews. Endocrinology. 2019;15(5):261-73.
2. S G, Cs W, B H, Vr J. Regulation of Intestinal Barrier Function by Microbial Metabolites. Cellular and molecular gastroenterology and hepatology. 2021;11(5):1463-82.
3. Sy Z, Hx L, Rc X, Wt M, My D, St D, et al. Potential roles of gut microbiota and microbial metabolites in Parkinson's disease. Ageing Res Rev. 2021;69:101347.
4. Cg B, Eg P. Microbiota-mediated colonization resistance against intestinal pathogens. Nature reviews. Immunology. 2013;13(11):790-801.
5. A A, J C, Pa B, F V, de Gunzburg J. Spare and repair the gut microbiota from antibiotic-induced dysbiosis: state-of-the-art. In. 26; 2021; 2159-63.
6. Hj F, Kp S, P L, Sh D. The role of the gut microbiota in nutrition and health. Nature reviews. Gastroenterology & hepatology. 2012;9(10):577-89.
7. M W, Tl W, Sl H. Gut Microbiota and Cardiovascular Disease. Circ Res. 2020;127(4):553-70.
8. Lh N, Ak Ö, Y C, Tg S, B R, M S, et al. Antibiotic use and the development of inflammatory bowel disease: a national case-control study in Sweden. In. 5; 2020; 986-95.
9. D A, Sf O, T O, Jf N, Fy A, D E, et al. Sphingolipids from a symbiotic microbe regulate homeostasis of host intestinal natural killer T cells. In. 156; 2014; 123-33.
10. Mp F. Antibiotics and the Human Gut Microbiome: Dysbioses and Accumulation of Resistances. In. 6; 2015; 1543.
11. Jd D. Pig vaccination strategies based on enterotoxigenic Escherichia coli toxins. Brazilian journal of microbiology: [publication of the Brazilian Society for Microbiology]. 2021;52(4):2499-509.
12. H Y, X D, L S, X Z, H L, N L, et al. Protective Ability of Biogenic Antimicrobial Peptide Microcin J25 Against Enterotoxigenic Escherichia Coli -Induced Intestinal Epithelial Dysfunction and Inflammatory Responses IPEC-J2 Cells. Front Cell Infect Mi. 2018;8:242.
13. Rj C, Dt R. Fecal microbiota transplantation as therapy for inflammatory bowel disease: a systematic review and meta-analysis. Journal of Crohn's & colitis. 2014;8(12):1569-81.
14. Tj B, Gd E, Rl C. Fecal microbiota transplantation as a new therapy: from Clostridioides difficile infection to inflammatory bowel disease, irritable bowel syndrome, and colon cancer. Curr Opin Pharmacol. 2019;49:43-51.
15. S C, X M, S G, X J, Y L, L H, et al. Fecal Microbiota Transplantation Beneficially Regulates Intestinal Mucosal Autophagy and Alleviates Gut Barrier Injury. Msystems. 2018;3(5).
16. Mf S, Yl Z, Zl Z, Xb J, Yd X, Q Y, et al. Neuroprotective effects of fecal microbiota transplantation on MPTP-induced Parkinson's disease mice: Gut microbiota, glial reaction and TLR4/TNF-α signaling pathway. Brain, behavior, and immunity. 2018;70:48-60.
17. Mn Q, M W, N B, D M, M P, N S, et al. Systematic review with meta-analysis: the efficacy of faecal microbiota transplantation for the treatment of recurrent and refractory Clostridium difficile infection. Aliment Pharm Ther. 2017;46(5):479-93.
18. X M, T X, M Q, Y Z, Z Y, X H. Faecal microbiota transplantation alleviates early-life antibiotic-induced gut microbiota dysbiosis and mucosa injuries in a neonatal piglet model. Microbiol Res. 2021;255:126942.
19. Jm W, Rj B, M D, Tt M, F T, Pd C, et al. Homeostasis of the gut barrier and potential biomarkers. American journal of physiology. Gastrointestinal and liver physiology. 2017;312(3):G171-93.

20. Jm M, Jb M. Mucosal repair in the gastrointestinal tract. Crit Care Med. 2003;31(8 Suppl):S532-7.
21. N B, van Es JH, J K, P K, van den Born M, M C, et al. Identification of stem cells in small intestine and colon by marker gene Lgr5. Nature. 2007;449(7165):1003-7.
22. Ks Y, Cy J, J C, Gxy Z, Ka L, Vc L, et al. Non-equivalence of Wnt and R-spondin ligands during Lgr5 + intestinal stem-cell self-renewal. Nature. 2017;545(7653):238-42.
23. T S, Rg V, Hj S, van de Wetering M, N B, De S, et al. Single Lgr5 stem cells build crypt-villus structures in vitro without a mesenchymal niche. Nature. 2009;459(7244):262-5.
24. J S, Ic Z, Mm M. Organoid-based modeling of intestinal development, regeneration, and repair. Cell Death Differ. 2021;28(1):95-107.
25. Yb Y, Sg G, D W, X W, Yl Y. Enteroids: Promising in Vitro Models for Studies of Intestinal Physiology and Nutrition in Farm Animals. J Agr Food Chem. 2019;67(9):2421-8.
26. Jy C, M M, X L, At M, Cj K, Dm M, et al. Controlling Epithelial Polarity: A Human Enteroid Model for Host-Pathogen Interactions. Cell Rep. 2019;26(9):2509-20.
27. Hb K, Re I. The pig gut microbial diversity: Understanding the pig gut microbial ecology through the next generation high throughput sequencing. Vet Microbiol. 2015;177(3-4):242-51.
28. Jy C, M M, Dm M, Mr A. Controlling the polarity of human gastrointestinal organoids to investigate epithelial biology and infectious diseases. Nat Protoc. 2021;16(11):5171-92.
29. Xie Z, Li M, Qian M, Yang Z, Han X. Co-Cultures of Lactobacillus acidophilus and Bacillus subtilis Enhance Mucosal Barrier by Modulating Gut Microbiota-Derived Short-Chain Fatty Acids. Nutrients. 2022;14(21):4475.
30. H Y, X D, L S, X Z, H L, N L, et al. Protective Ability of Biogenic Antimicrobial Peptide Microcin J25 Against Enterotoxigenic Escherichia Coli -Induced Intestinal Epithelial Dysfunction and Inflammatory Responses IPEC-J2 Cells. Front Cell Infect Mi. 2018;8:242.
31. X M, T X, M Q, Y Z, Z Y, X H. Faecal microbiota transplantation alleviates early-life antibiotic-induced gut microbiota dysbiosis and mucosa injuries in a neonatal piglet model. Microbiol Res. 2021;255:126942.
32. Y S, Sw K. Intestinal challenge with enterotoxigenic Escherichia coli in pigs, and nutritional intervention to prevent postweaning diarrhea. Animal nutrition (Zhongguo xu mu shou yi xue hui). 2017;3(4):322-30.
33. W X, L S, X W, Y X, Z L, D Z, et al. A bovine lactoferricin-lactoferrampin-encoding Lactobacillus reuteri CO21 regulates the intestinal mucosal immunity and enhances the protection of piglets against enterotoxigenic Escherichia coli K88 challenge. Gut microbes. 2021;13(1):1956281.
34. W W, Y W, X H, Y D, Z M, X A, et al. Dietary fermented soybean meal replacement alleviates diarrhea in weaned piglets challenged with enterotoxigenic Escherichia coli K88 by modulating inflammatory cytokine levels and cecal microbiota composition. Bmc Vet Res. 2020;16(1):245.
35. S G, S C, Y L, Z W, X M, X J, et al. Faecal Microbiota Transplantation Reduces Susceptibility to Epithelial Injury and Modulates Tryptophan Metabolism of the Microbial Community in a Piglet Model. Journal of Crohn's & colitis. 2018;12(11):1359-74.
36. Q L, P K, Tj V, A S, Wg L, Da R, et al. Enterotoxigenic Escherichia coli secretes a highly conserved mucin-degrading metalloprotease to effectively engage intestinal epithelial cells. Infect Immun. 2014;82(2):509-21.
37. Kr B, Sx L, R T, A K, Jr T, Hl L, et al. Bifidobacteria stabilize claudins at tight junctions and prevent intestinal barrier dysfunction in mouse necrotizing enterocolitis. The American journal of pathology. 2013;182(5):1595-606.
38. C C, J G, Sh R. Mechanisms regulating intestinal barrier integrity and its pathological implications.

769 Experimental & molecular medicine. 2018;50(8):1-9.
770 39. Y H, J W, G Q, X W, L Y, L Z. Lactobacillus acidophilus ATCC 4356 prevents atherosclerosis via
771 inhibition of intestinal cholesterol absorption in apolipoprotein E-knockout mice. Appl Environ Microb.
772 2014;80(24):7496-504.
773 40. Sn C, Cj D, C H, G D. Role of ompR-dependent genes in Salmonella typhimurium virulence: mutants
774 deficient in both ompC and ompF are attenuated in vivo. Infect Immun. 1991;59(1):449-52.
775 41. M W, B W, Km K, A M, Ks B, N G, et al. Antibiotic treatment alters the colonic mucus layer and
776 predisposes the host to exacerbated Citrobacter rodentium-induced colitis. Infect Immun. 2011;79(4):1536-
777 45.
778 42. N O, J R, M M, Te P, V K, J K, et al. Pili-like proteins of Akkermansia muciniphila modulate host immune
779 responses and gut barrier function. Plos One. 2017;12(3):e173004.
780 43. C B, de Vos WM. Microbes inside--from diversity to function: the case of Akkermansia. The ISME journal.
781 2012;6(8):1449-58.
782 44. J C, M J, B K, Ds N, Lh H, Bc S, et al. Treatment with a Monoclonal Anti-IL-12p40 Antibody Induces
783 Substantial Gut Microbiota Changes in an Experimental Colitis Model. Gastroent Res Pract.
784 2016;2016:4953120.
785 45. H P, A E, C D, C D, Van Hul M, L G, et al. A purified membrane protein from Akkermansia muciniphila
786 or the pasteurized bacterium improves metabolism in obese and diabetic mice. Nat Med. 2017;23(1):107-13.
787 46. A E, C B, L G, Jp O, C D, Lb B, et al. Cross-talk between Akkermansia muciniphila and intestinal
788 epithelium controls diet-induced obesity. P Natl Acad Sci Usa. 2013;110(22):9066-71.
789 47. J L, S L, Pm V, Cw W, A X. Akkermansia Muciniphila Protects Against Atherosclerosis by Preventing
790 Metabolic Endotoxemia-Induced Inflammation in Apoe-/- Mice. Circulation. 2016;133(24):2434-46.
791 48. L Z, Q Q, M L, X Z, F H, G W. Akkermansia muciniphila can reduce the damage of gluco/lipotoxicity,
792 oxidative stress and inflammation, and normalize intestine microbiota in streptozotocin-induced diabetic
793 rats. Pathog Dis. 2018;76(4).
794 49. Ey H, Sw M, S H, G S, Er H, T M, et al. Microbiota modulate behavioral and physiological abnormalities
795 associated with neurodevelopmental disorders. Cell. 2013;155(7):1451-63.
796 50. Gp D, Sm L, Sk M. Gut biogeography of the bacterial microbiota. Nature reviews. Microbiology.
797 2016;14(1):20-32.
798 51. H D, Z L, Y T, Z G, Y L, Y W, et al. A novel strain of Bacteroides fragilis enhances phagocytosis and
799 polarises M1 macrophages. Sci Rep-Uk. 2016;6:29401.
800 52. X B, W W, L Y, L L, Q W, Y L, et al. Administration of Akkermansia muciniphila Ameliorates Dextran
801 Sulfate Sodium-Induced Ulcerative Colitis in Mice. Front Microbiol. 2019;10:2259.
802 53. R Z, X X, L Z, X Y, L Z, C Z. Strain-Specific Anti-inflammatory Properties of Two Akkermansia
803 muciniphila Strains on Chronic Colitis in Mice. Front Cell Infect Mi. 2019;9:239.
804 54. C W, S L, K H, L Y, F T, J Z, et al. The roles of different Bacteroides fragilis strains in protecting against
805 DSS-induced ulcerative colitis and related functional genes. Food Funct. 2021.
806 55. Y Z, L W, Jp Z, Jy Y, Zm Z, Xy Z. Expression of p53, c-erbB-2 and Ki67 in intestinal metaplasia and
807 gastric carcinoma. World J Gastroentero. 2010;16(3):339-44.
808 56. Q H, Y D, Q Y, B W, Le S, Y G, et al. Regulation of the Paneth cell niche by exogenous L-arginine
809 couples the intestinal stem cell function. FASEB journal: official publication of the Federation of American
810 Societies for Experimental Biology. 2020;34(8):10299-315.
811 57. A R, Ym K, M K. Wnt/catenin signaling in adult stem cell physiology and disease. Stem Cell Rev Rep.

812 2014;10(4):512-25.
813 58. C N. The complex world of WNT receptor signalling. Nature reviews. Molecular cell biology.
814 2012;13(12):767-79.
815 59. Y S, B S, R Y, Y X, B X, J L, et al. Wnt and Notch signaling pathway involved in wound healing by
816 targeting c-Myc and Hes1 separately. Stem Cell Res Ther. 2015;6:120.
817 60. Jy Z, Dg H, Cq G, Hc Y, Sg Z, Xq W. Heat-stable enterotoxin inhibits intestinal stem cell expansion to
818 disrupt the intestinal integrity by downregulating the Wnt/ β -catenin pathway. Stem cells (Dayton, Ohio).
819 2021;39(4):482-96.
820 61. Y L, N Y, J C, X H, N Z, S Y, et al. Next-Generation Porcine Intestinal Organoids: an Apical-Out Organoid
821 Model for Swine Enteric Virus Infection and Immune Response Investigations. J Virol. 2020;94(21).
822 62. D S, Drg P, A B, Mn F, Ka H, C C, et al. The Development of Ovine Gastric and Intestinal Organoids for
823 Studying Ruminant Host-Pathogen Interactions. Front Cell Infect Mi. 2021;11:733811.
824 63. Tj N, Km M, Na M, L V. Inside-out chicken enteroids with leukocyte component as a model to study host-
825 pathogen interactions. Communications biology. 2021;4(1):377.
826
827

Figure legends:

Figure 1. Experimental designs of the present study. (A) Schematic diagram of the FMT administered to the AIMD piglets infected with ETEC K88. (B) Schematic diagram of the alleviatory effects of *A. muciniphila* and *B. fragilis* on ETEC K88 infection in mice. (C) Schematic diagram of the alleviatory effects of *A. muciniphila* on ETEC K88 infection in porcine basal-out and apical-out intestinal organoids.

Figure 2. FMT improved the intestinal morphology and barrier function in AIMD piglets infected with ETEC K88. (A) SEM images of villi (top) and microvilli (bottom) in the jejunum (scale bars = 300 or 2 μm). (B) The relative mRNA expression of tight junction proteins (ZO-1, claudin and occludin) and adheren junctions (β-catenin and E-cadherin) in the jejunum. (C) The relative protein expression of tight junction proteins (ZO-1, claudin and occludin) and adheren junction proteins (β-catenin and E-cadherin) in the jejunum. (D) Immunofluorescence images of Mucin 2 (MUC2, green) in the jejunum (scale bars = 50 μm). Con: control group, EP: ETEC K88 + PBS group, EF: ETEC K88 + FMT group. Data are expressed as the mean ± SD. *, $P < 0.05$, **, $P < 0.01$. Data shown are representative of at least two independent experiments.

Figure 3. FMT changed the composition of gut microbiota and the concentration of SCFAs in AIMD piglets infected with ETEC K88. (A) Anosim analysis. (B) UPGMA clustering analysis based on Unweighted unifrac distance. (C) LEfSe analysis with LDA score > 4. (D) Quantification of SCFA metabolites (acetic acid, propionic acid, butyric acid, isobutyric acid, isovaleric acid and hexanoic acid). EP: ETEC K88 + PBS group, EF: ETEC K88 + FMT group. Data are expressed as the mean ± SD. *, $P < 0.05$, **, $P < 0.01$. Data shown are representative of at least two independent experiments.

Figrue 4. *A. muciniphila* and *B. fragilis* improved the intestinal morphology of mice infected with ETEC K88. (A) H&E-stained images of jejunum (scale bars = 50 μm) and the histograms of villus height, crypt depth and the ratio of villus height to crypt depth. (B) TEM images of jejunum and colon (scale bars = 0.5 μm). (C) PAS-stained images of colon (scale bars = 50 μm) and the histogram of crypt depth and number of goblet cell. (D) Immunofluorescence images of Mucin 2 (MUC2, green) in the jejunum and colon (scale bars = 50 μm). C: control group, E: ETEC K88 + PBS group, A: ETEC K88 + *A. muciniphila* group, B: ETEC K88 + *B. fragilis* group. Data are expressed as the mean ± SD. *, $P < 0.05$, **, $P < 0.01$, ***, $P < 0.001$. Data shown are representative of at least two independent experiments.

Figure 5. *A. muciniphila* and *B. fragilis* regulated the expression of inflammatory cytokines and the balance of Treg and Th17 cells in mice infected with ETEC K88. (A) The relative mRNA expression of cytokines in the jejunum. (B) Flow cytometric dot plots and proportions of Treg ($CD25^+Foxp3^+$), Th17 ($CD4^+ROR\gamma t^+$) and mature dendritic cells ($CD86^+CD11C^+$) in jejunal lamina propria. C: control group, E: ETEC K88 + PBS group, A: ETEC K88 + *A. muciniphila* group, B: ETEC K88 + *B. fragilis* group. Data are expressed as the mean ± SD. *, $P < 0.05$, **, $P < 0.01$, ***, $P < 0.001$. Data shown are representative of at least two independent experiments.

Figure 6. *A. muciniphila* and *B. fragilis* enhanced the number of Ki67 cells and Lyz Paneth cells in jejunal crypt of mice infected with ETEC K88 by moderately activating the Wnt/β-catenin pathway. (A) The mRNA expression and immunofluorescence staining images of intestinal epithelial cell proliferation marker Ki67 (red). (B) The mRNA expression and immunofluorescence staining images of Paneth marker Lyz (green). (C) The relative mRNA expression of *Lgr5*, *Wnt3*, *Notch1* and other genes in jejunum mucosa. (D) The relative protein expression of Wnt/β-catenin pathway and its target genes in jejunum mucosa. C: control group, E: ETEC K88 + PBS group, A: ETEC K88 + *A. muciniphila* group, B:

ETEC K88 + *B. fragilis* group. Data are expressed as the mean ± SD. *, $P < 0.05$, **, $P < 0.01$, ***, $P < 0.001$. Data shown are representative of at least two independent experiments.

Figure 7. *A. muciniphila* and *B. fragilis* promoted the activity of Lgr5$^+$ intestinal stem cells as proved by the growth of intestinal organoids. (A) Morphology of *ex vivo* culture of crypts isolated from the jejunum of mice in the C, E, A and B groups (Day 5; 4 ×, scale bars = 200 μm; 20 ×, scale bars = 50 μm). (B) The surface area and forming efficiency of intestinal organoids. (C) The relative mRNA expression of genes related to the proliferation and differentiation of the intestinal organoids. C: control group, E: ETEC K88 + PBS group, A: ETEC K88 + *A. muciniphila* group, B: ETEC K88 + *B. fragilis* group. Data are expressed as the mean ± SD. *, $P < 0.05$, **, $P < 0.01$, ***, $P < 0.001$. Data shown are representative of at least two independent experiments.

Figure 8. *A. muciniphila* protected the Lgr5$^+$ intestinal stem cell and activated the Wnt/β-catenin signaling pathway of the ETEC K88-induced basal-out intestinal organoids. (A) The relative mRNA expression of *villin*, *ZO-1*, *Ki67*, *Lyz1*, *MUC2*, *Lgr5*, *Wnt3a* and *β-catenin* genes. (B)-(F) Immunofluorescence images of villin (scale bars = 50 μm), Ki67 (scale bars = 50 μm), Lgr5 (scale bars = 20 μm), Wnt3a (scale bars = 50 μm) and β-catenin (scale bars = 50 μm). (G) Fold change of the mean fluorescence intensity. CON: control group, ETEC: ETEC K88 + DMEM/F-12 group, AKK: ETEC K88 + *A. muciniphila* group, WNT-C59: Wnt-C59 + ETEC K88 + *A. muciniphila* group. Data are expressed as the mean ± SD. *, $P < 0.05$, **, $P < 0.01$, ***, $P < 0.001$. Data shown are representative of at least two independent experiments.

Figure 9. *A. muciniphila* alleviated the intestinal epithelial injury of the ETEC K88-induced apical-out intestinal organoids. (A) Confocal microscope visualization of the apical-out intestinal organoids incubated in FD4 solution (scale bars = 50 μm). (B) The relative mRNA expression of *villin*, *ZO-1*, *Ki67*, *Lyz1*, *MUC2*, *Lgr5*, *Wnt3a* and *β-catenin* genes. (C)-(G) Immunofluorescence images of villin, Ki67, Lgr5, Wnt3a and β-catenin (scale bars = 20 μm). (H) Quantification of the apical-out intestinal organoids incubated in FD4 solution that have intact barrier integrity. (I) Fold change of the mean fluorescence intensity. (J) The relative mRNA expression of cytokines in the apical-out intestinal organoids. CON: control group, ETEC: ETEC K88 + DMEM/F-12 group, AKK: ETEC K88 + *A. muciniphila* group, WNT-C59: Wnt-C59 + ETEC K88 + *A. muciniphila* group. Data are expressed as the mean ± SD. *, $P < 0.05$, **, $P < 0.01$, ***, $P < 0.001$. Data shown are representative of at least two independent experiments.

900 **Figure 1**

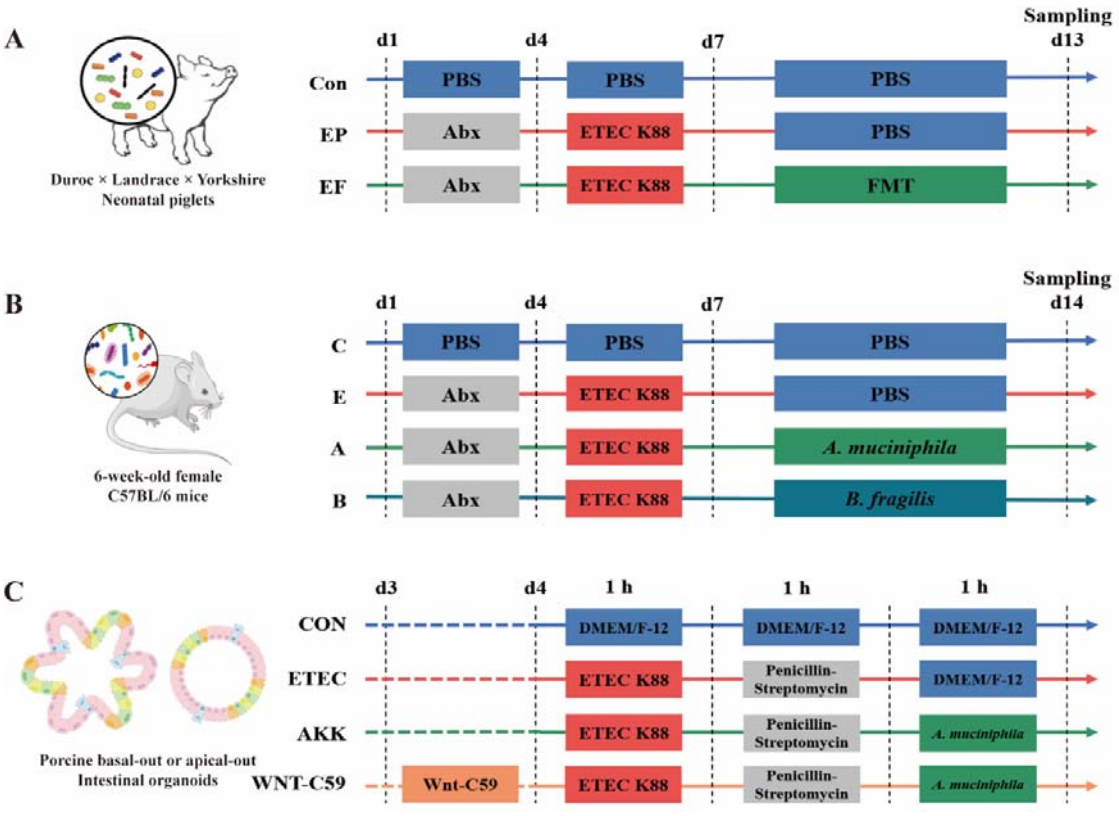

901

Figure 2

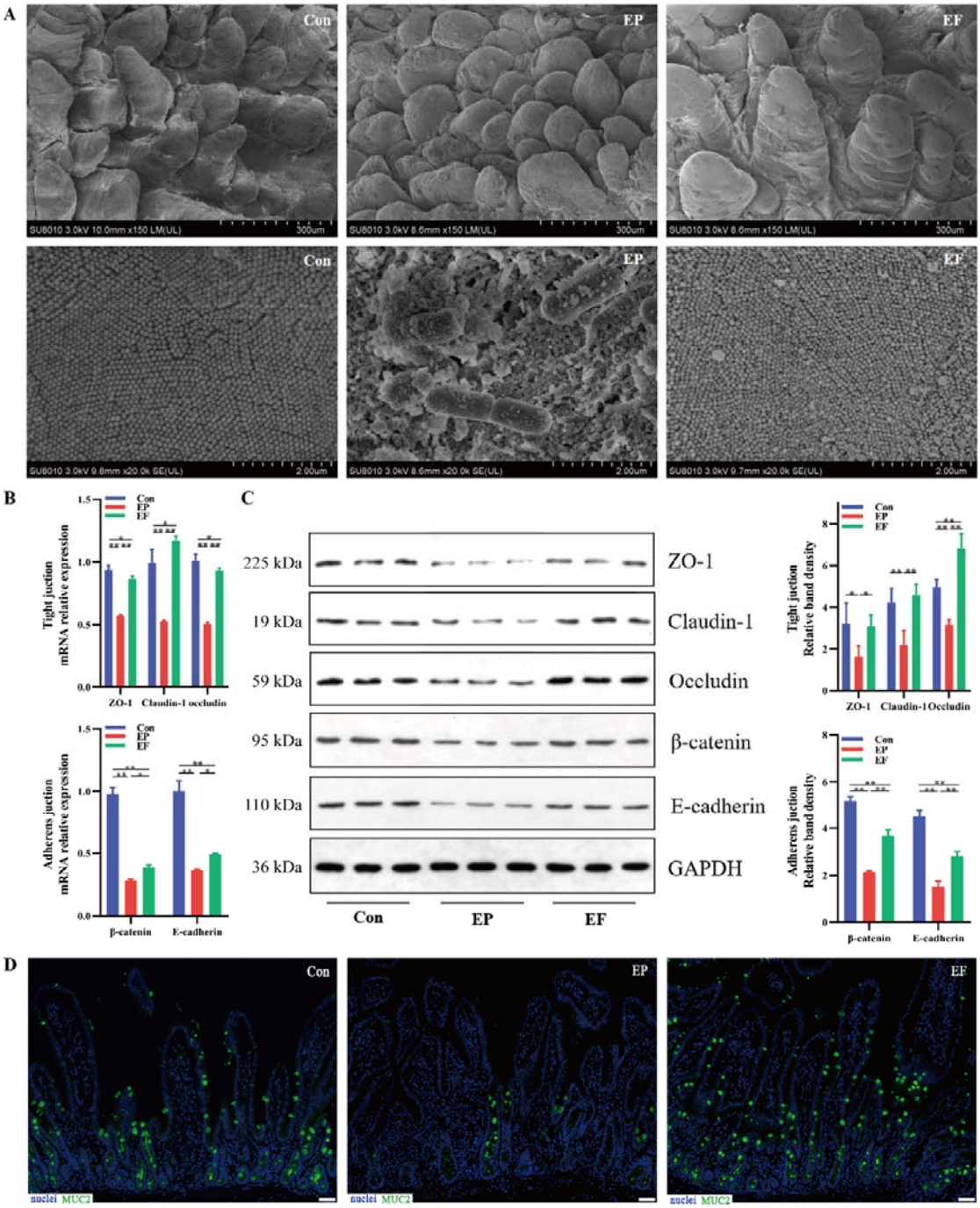
A
Con
EP
EF
B
Tight junction mRNA relative expression
ZO-1
Claudin-1
occludin
Adherens junction mRNA relative expression
β-catenin
E-cadherin
C
225 kDa
ZO-1
19 kDa
Claudin-1
59 kDa
Occludin
95 kDa
β-catenin
110 kDa
E-cadherin
36 kDa
GAPDH
Tight junction Relative band density
Adherens junction Relative band density
D
nuclei MUC2

Figure 3

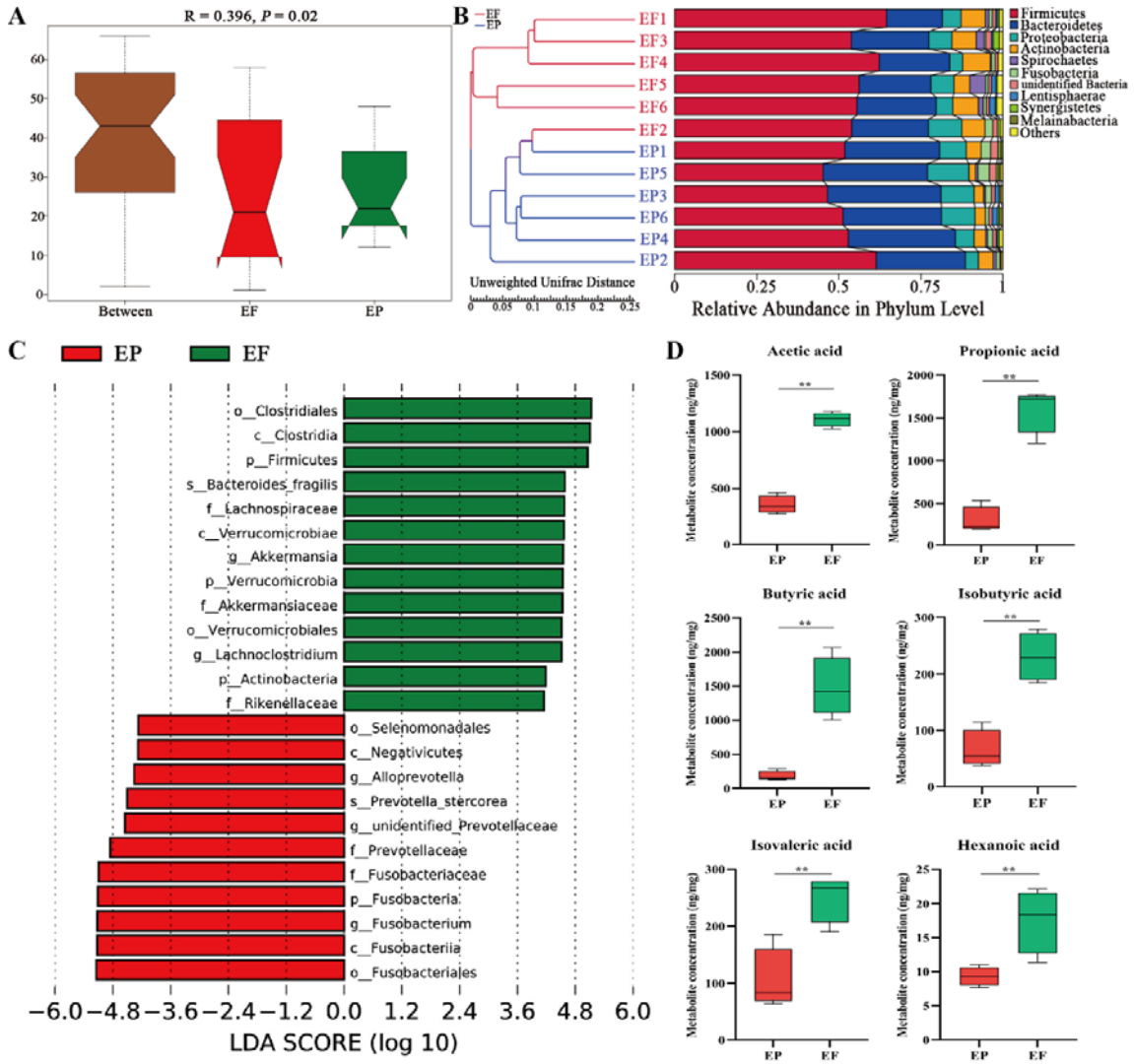
A
R = 0.396, P = 0.02
Between
EF
EP
B
EF
EP
EF1
EF3
EF4
EF5
EF6
EF2
EP1
EP5
EP3
EP6
EP4
EP2
Unweighted Unifrac Distance
Relative Abundance in Phylum Level
Firmicutes
Bacteroidetes
Proteobacteria
Actinobacteria
Spirochaetes
Fusobacteria
unidentified Bacteria
Lentisphaerae
Synergistetes
Melainabacteria
Others
C
EP
EF
o__Clostridiales
c__Clostridia
p__Firmicutes
s__Bacteroides_fragilis
f__Lachnospiraceae
c__Verrucomicrobiae
g__Akkermansia
p__Verrucomicrobia
f__Akkermansiaceae
o__Verrucomicrobiales
g__Lachnoclostridium
p__Actinobacteria
f__Rikenellaceae
o__Selenomonadales
c__Negativicutes
g__Alloprevotella
s__Prevotella_stercorea
g__unidentified_Prevotellaceae
f__Prevotellaceae
f__Fusobacteriaceae
p__Fusobacteria
g__Fusobacterium
c__Fusobacteriia
o__Fusobacteriales
LDA SCORE (log 10)
D
Acetic acid
Propionic acid
Butyric acid
Isobutyric acid
Isovaleric acid
Hexanoic acid
Metabolite concentration (ng/mg)
EP
EF

Figure 4

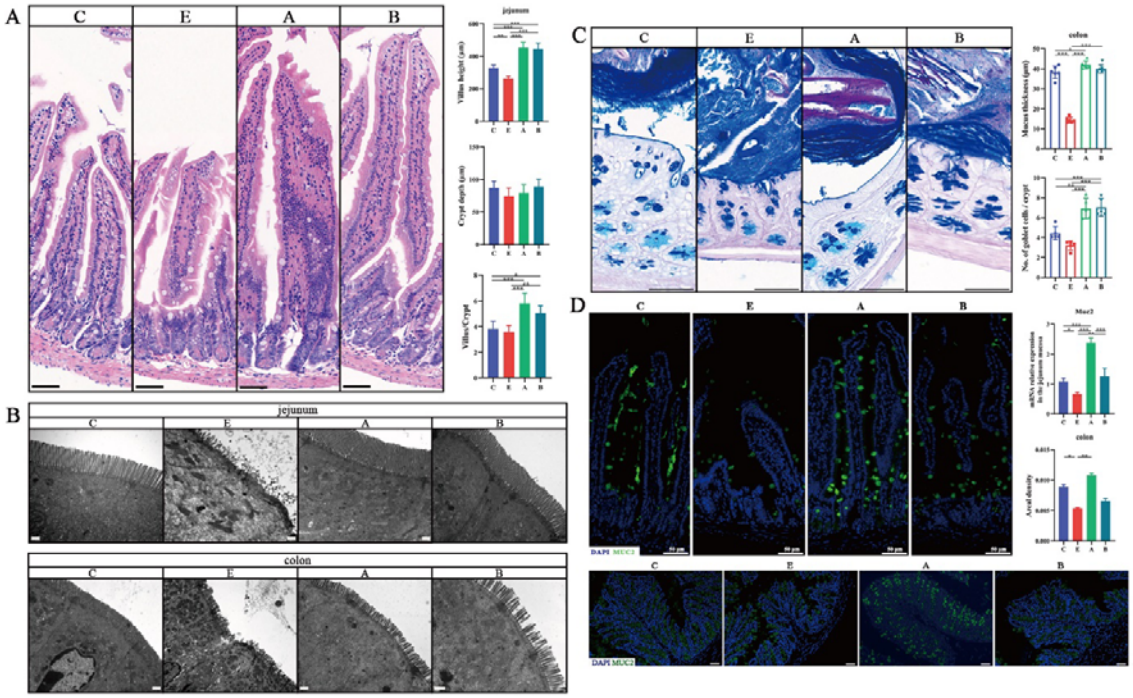
A
C
E
A
B
jejunum
Villus height (μm)
Crypt depth (μm)
Villus/Crypt
B
jejunum
colon
C
D
colon
Mucus thickness (μm)
No. of goblet cells / crypt
Muc2
colon
DAPI MUC2

Figure 5

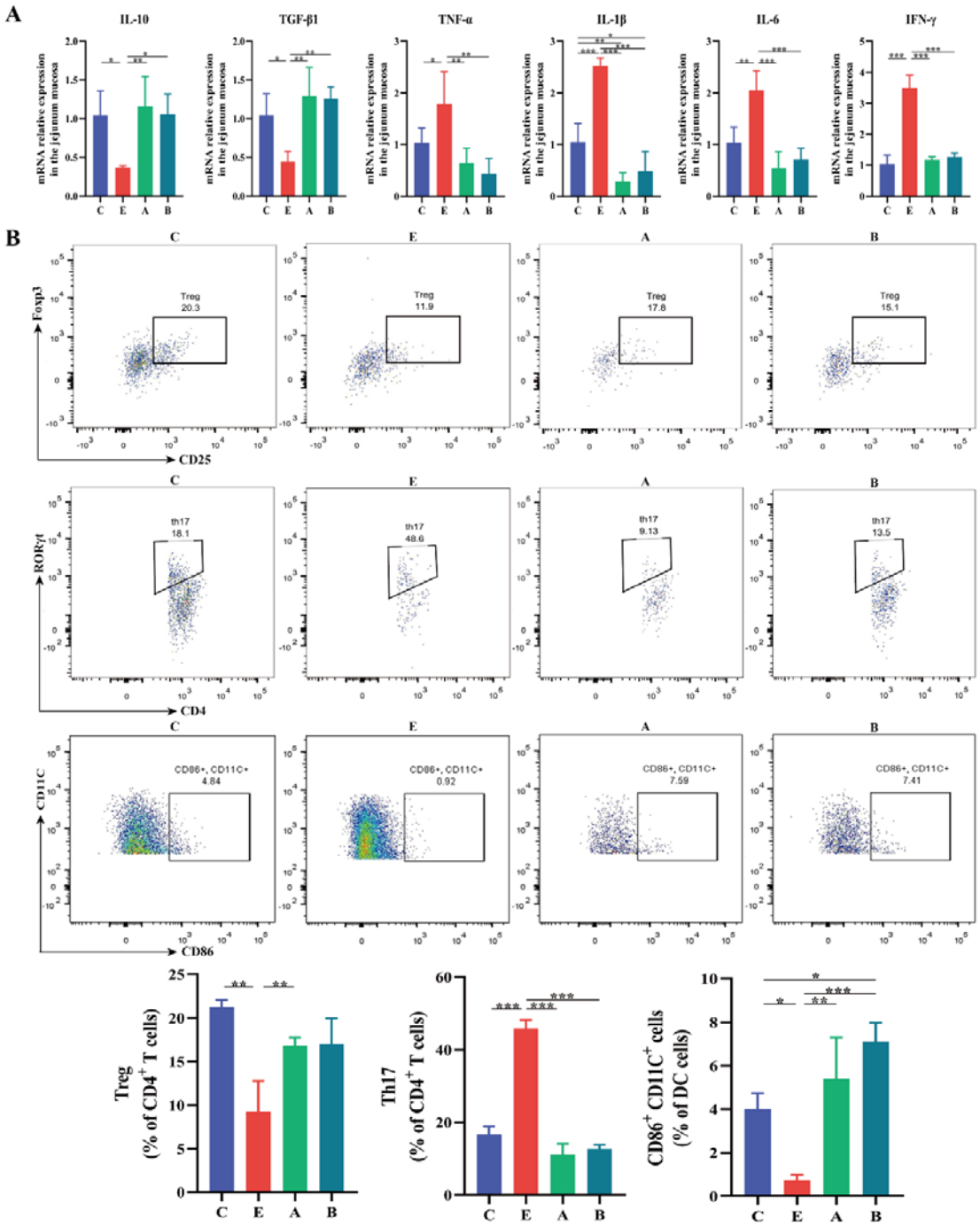
A
IL-10
TGF-β1
TNF-α
IL-1β
IL-6
IFN-γ
mRNA relative expression in the jejunum mucosa
C E A B
B
Foxp3
CD25
Treg 20.3
Treg 11.9
Treg 17.8
Treg 15.1
RORγt
CD4
th17 18.1
th17 48.6
th17 9.13
th17 13.5
CD11C
CD86
CD86+, CD11C+ 4.84
CD86+, CD11C+ 0.92
CD86+, CD11C+ 7.59
CD86+, CD11C+ 7.41
Treg (% of CD4+ T cells)
Th17 (% of CD4+ T cells)
CD86+ CD11C+ cells (% of DC cells)

Figure 6

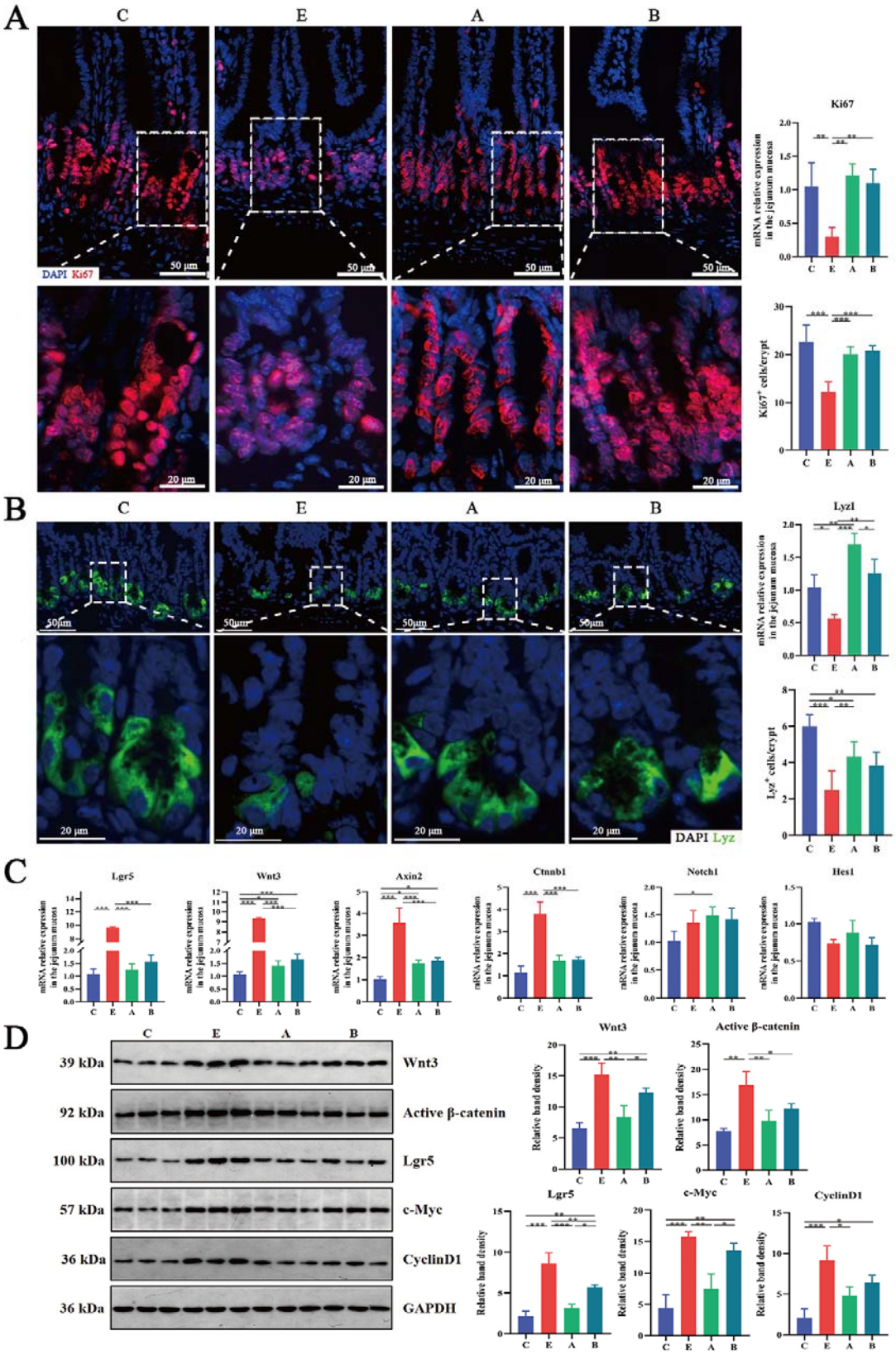
A
C
E
A
B
DAPI Ki67
50 μm
20 μm
Ki67
mRNA relative expression in the jejunum mucosa
Ki67+ cells/crypt
B
Lyz1
Lyz+ cells/crypt
DAPI Lyz
C
Lgr5
Wnt3
Axin2
Ctnnb1
Notch1
Hes1
mRNA relative expression in the jejunum mucosa
D
39 kDa
92 kDa
100 kDa
57 kDa
36 kDa
36 kDa
Wnt3
Active β-catenin
Lgr5
c-Myc
CyclinD1
GAPDH
Relative band density

913 **Figure 7**

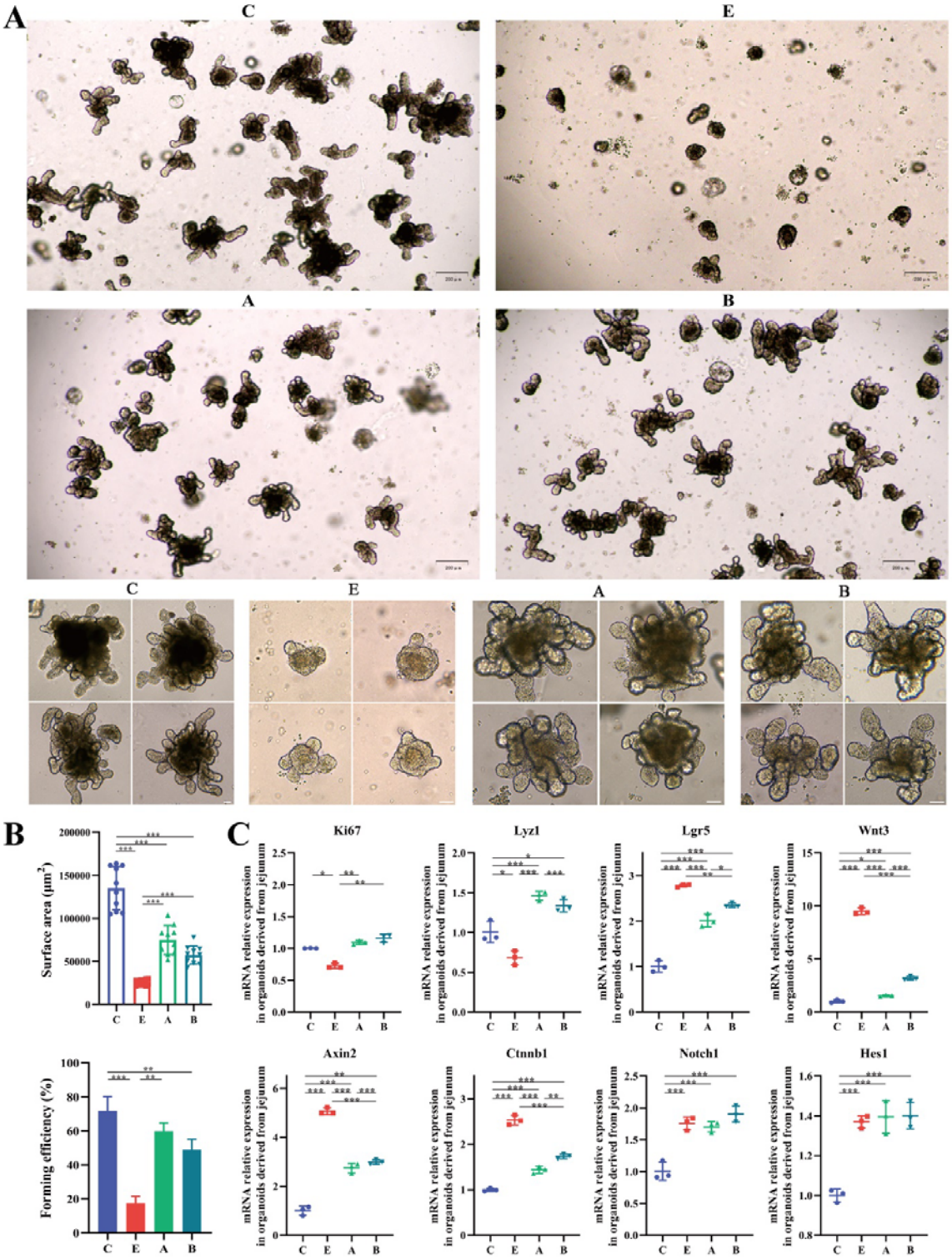

914

Figure 8

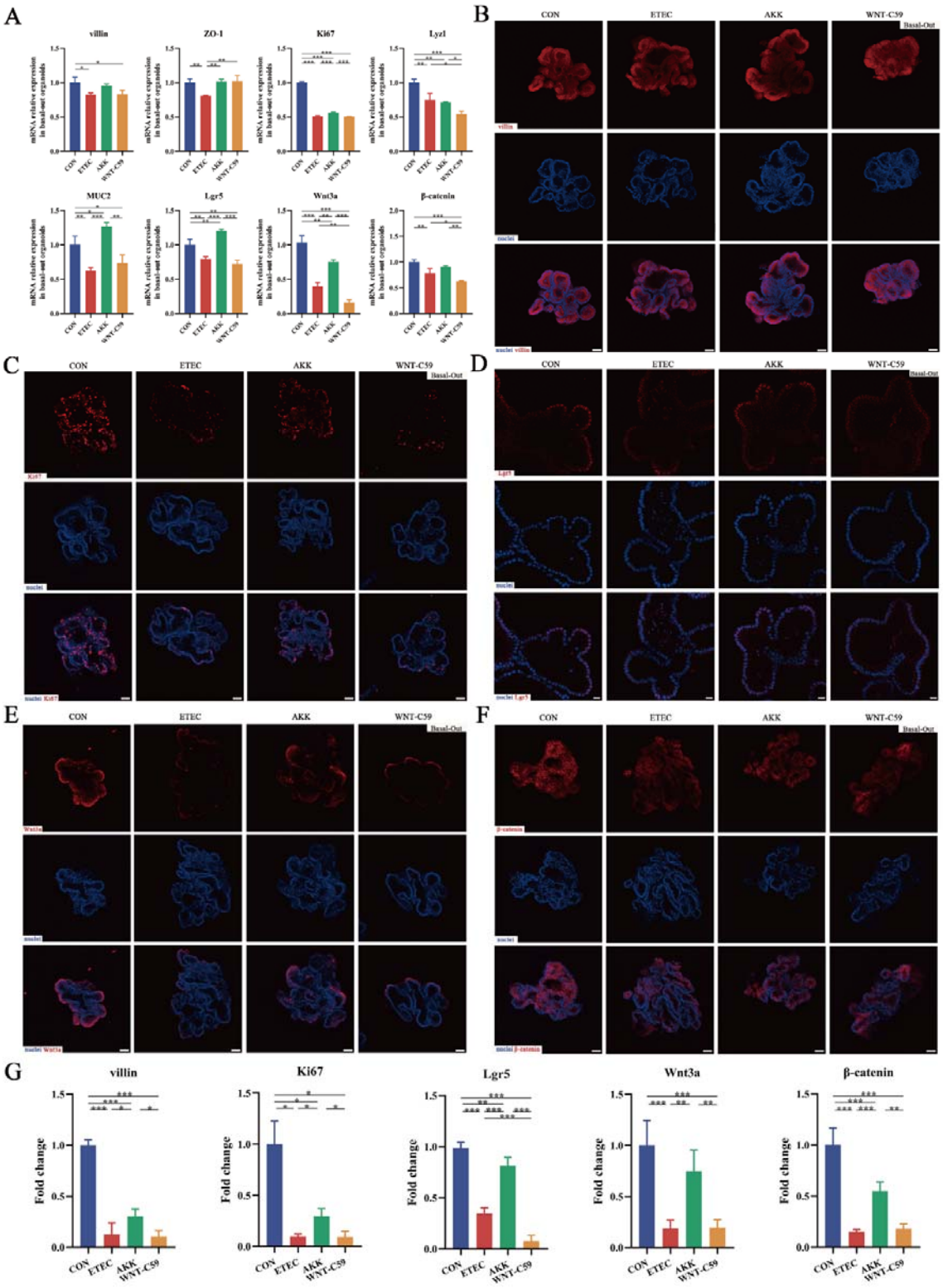
A
villin
ZO-1
Ki67
Lyz1
MUC2
Lgr5
Wnt3a
β-catenin
mRNA relative expression in basal-out organoids
CON
ETEC
AKK
WNT-C59
B
C
D
E
F
Basal-Out
villin
nuclei
Ki67
Lgr5
Wnt3a
β-catenin
G
Fold change

Figure 9

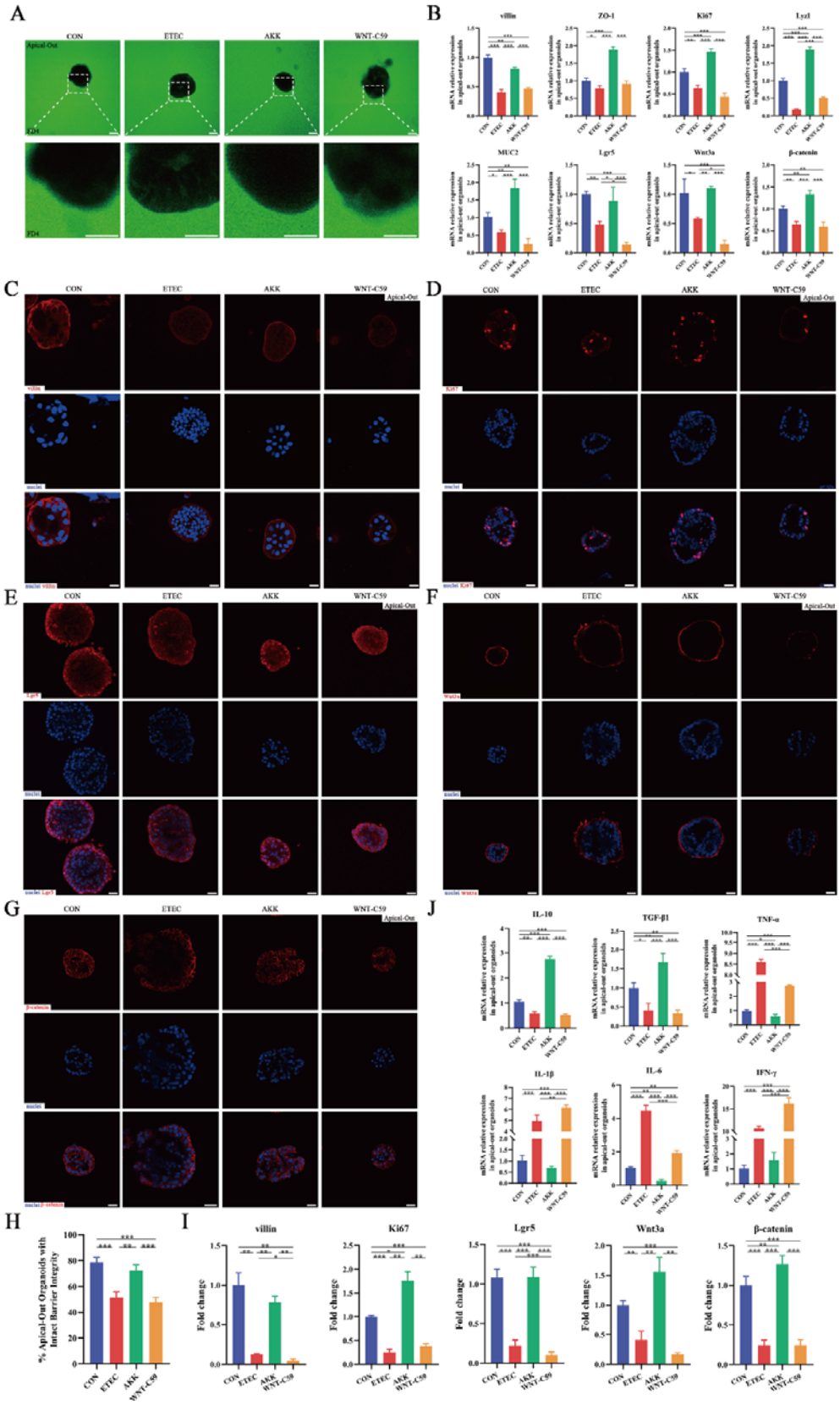
A
CON
ETEC
AKK
WNT-C59
Apical-Out
B
villin
ZO-1
Ki67
Lyzl
MUC2
Lgr5
Wnt3a
β-catenin
C
D
E
F
G
J
IL-10
TGF-β1
TNF-α
IL-1β
IL-6
IFN-γ
H
% Apical-Out Organoids with Intact Barrier Integrity
I
Fold change

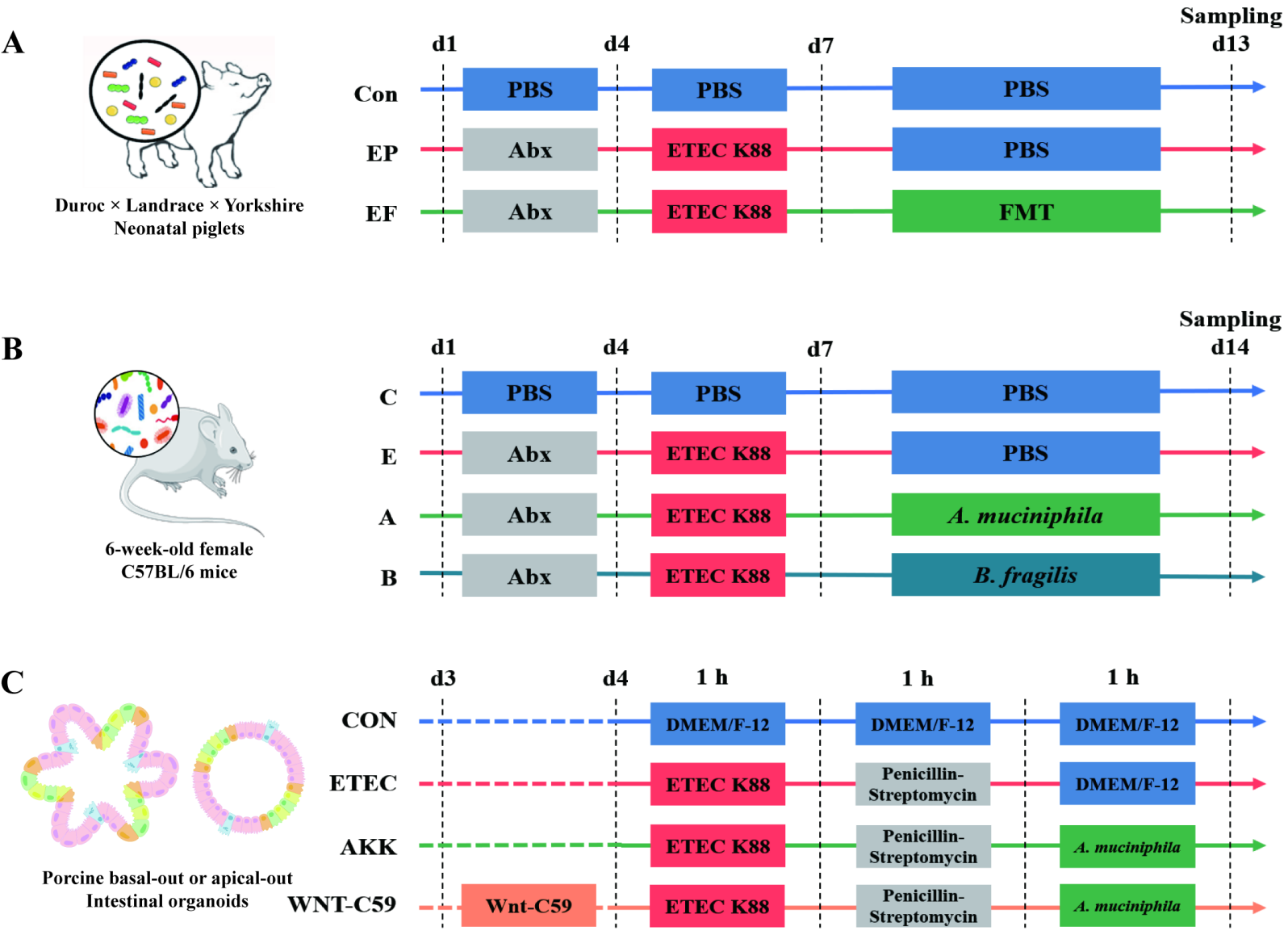
A
Duroc × Landrace × Yorkshire
Neonatal piglets
d1
d4
d7
Sampling
d13
Con
PBS
PBS
PBS
EP
Abx
ETEC K88
PBS
EF
Abx
ETEC K88
FMT
B
6-week-old female
C57BL/6 mice
d1
d4
d7
Sampling
d14
C
PBS
PBS
PBS
E
Abx
ETEC K88
PBS
A
Abx
ETEC K88
A. muciniphila
B
Abx
ETEC K88
B. fragilis
C
Porcine basal-out or apical-out
Intestinal organoids
d3
d4
1 h
1 h
1 h
CON
DMEM/F-12
DMEM/F-12
DMEM/F-12
ETEC
ETEC K88
Penicillin-Streptomycin
DMEM/F-12
AKK
ETEC K88
Penicillin-Streptomycin
A. muciniphila
WNT-C59
Wnt-C59
ETEC K88
Penicillin-Streptomycin
A. muciniphila

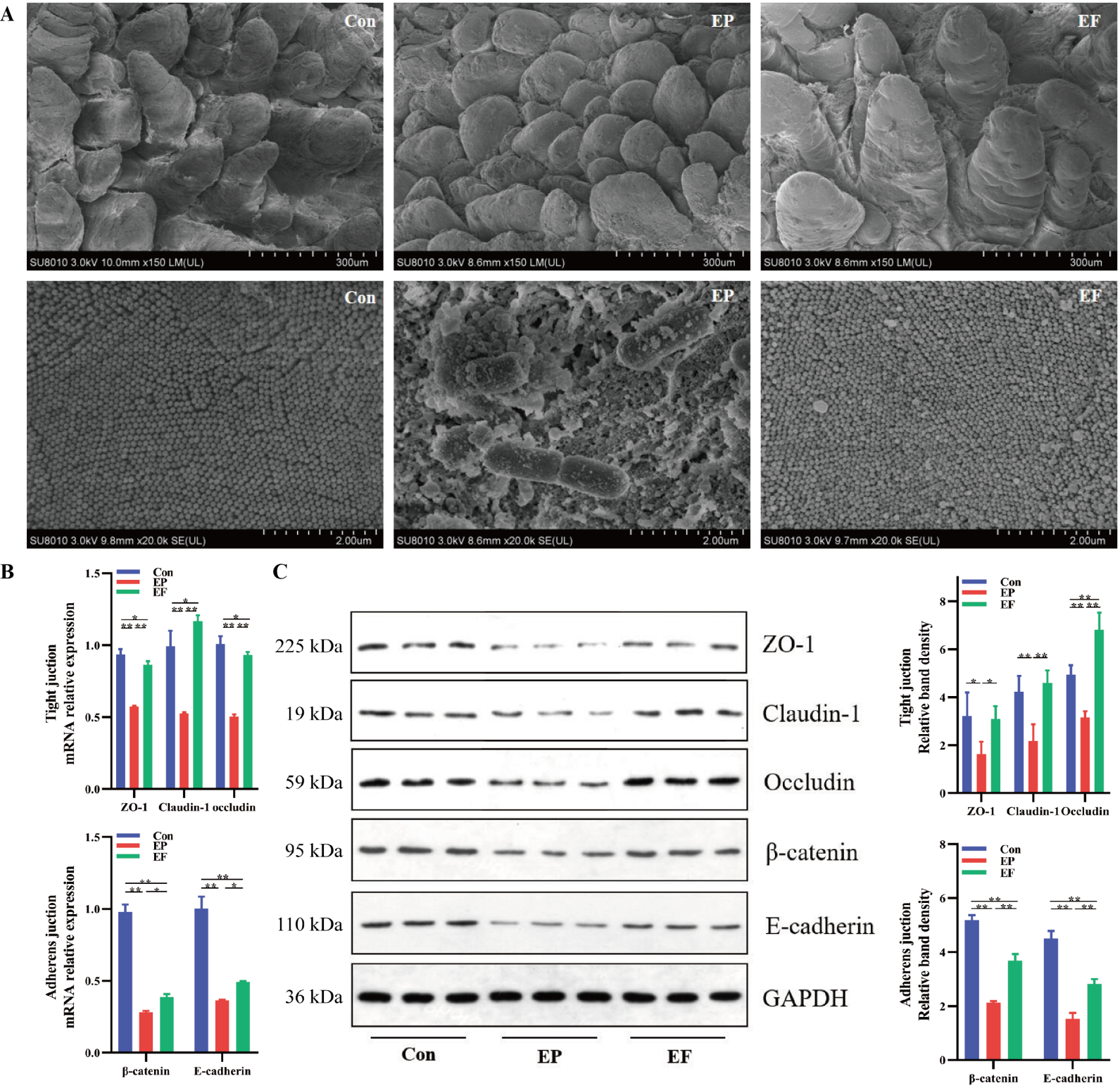
A
Con
EP
EF
SU8010 3.0kV 10.0mm x150 LM(UL)
300um
SU8010 3.0kV 8.6mm x150 LM(UL)
300um
SU8010 3.0kV 8.6mm x150 LM(UL)
300um
SU8010 3.0kV 9.8mm x20.0k SE(UL)
2.00um
SU8010 3.0kV 8.6mm x20.0k SE(UL)
2.00um
SU8010 3.0kV 9.7mm x20.0k SE(UL)
2.00um
B
Tight juction mRNA relative expression
ZO-1
Claudin-1
occludin
Adherens juction mRNA relative expression
β-catenin
E-cadherin
C
225 kDa
19 kDa
59 kDa
95 kDa
110 kDa
36 kDa
ZO-1
Claudin-1
Occludin
β-catenin
E-cadherin
GAPDH
Con
EP
EF
Tight juction Relative band density
Adherens juction Relative band density
D
nuclei MUC2

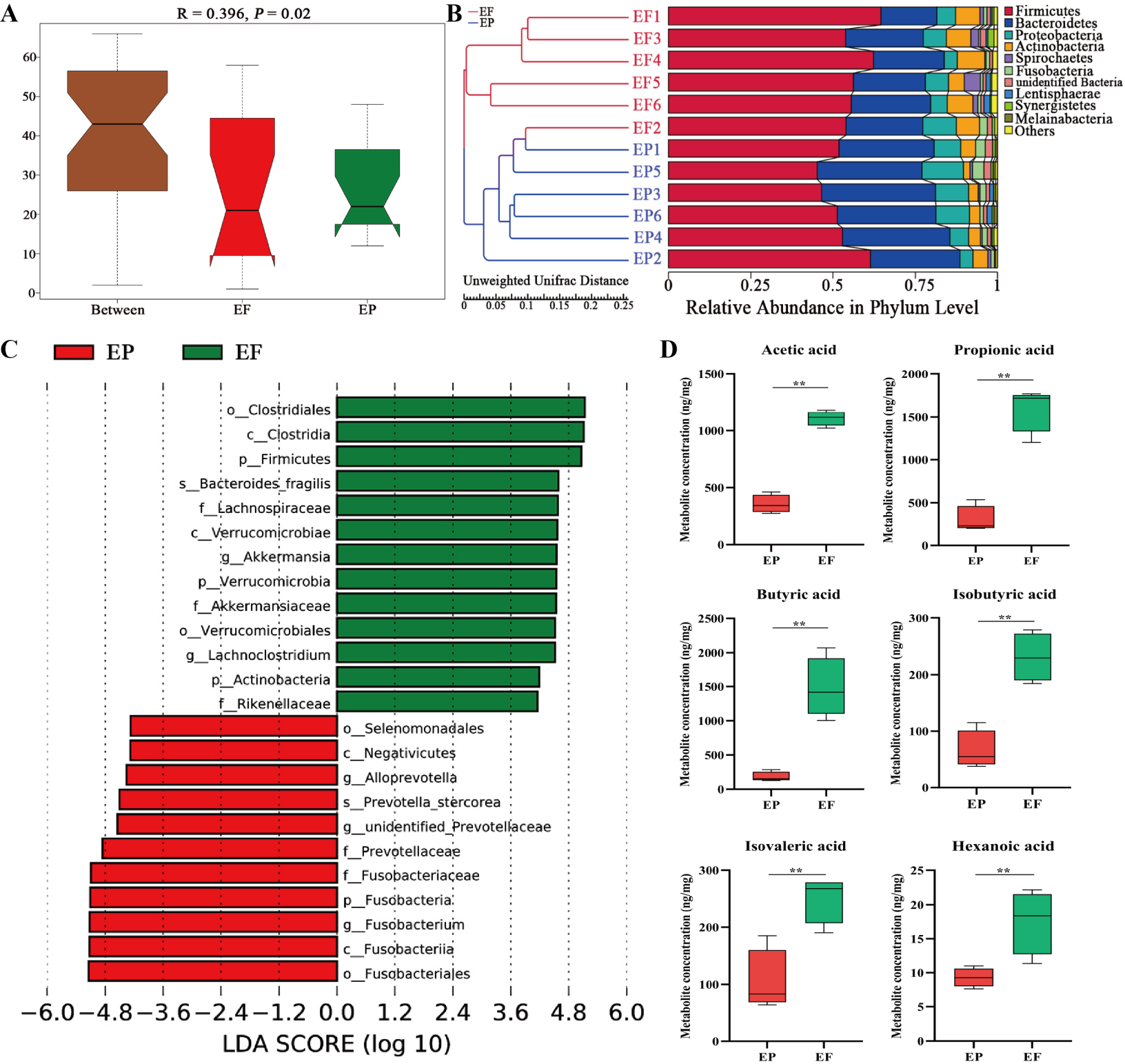
A
R = 0.396, P = 0.02
Between
EF
EP
B
EF
EP
EF1
EF3
EF4
EF5
EF6
EF2
EP1
EP5
EP3
EP6
EP4
EP2
Unweighted Unifrac Distance
Relative Abundance in Phylum Level
Firmicutes
Bacteroidetes
Proteobacteria
Actinobacteria
Spirochaetes
Fusobacteria
unidentified Bacteria
Lentisphaerae
Synergistetes
Melainabacteria
Others
C
EP
EF
o__Clostridiales
c__Clostridia
p__Firmicutes
s__Bacteroides_fragilis
f__Lachnospiraceae
c__Verrucomicrobiae
g__Akkermansia
p__Verrucomicrobia
f__Akkermansiaceae
o__Verrucomicrobiales
g__Lachnoclostridium
p__Actinobacteria
f__Rikenellaceae
o__Selenomonadales
c__Negativicutes
g__Alloprevotella
s__Prevotella_stercorea
g__unidentified_Prevotellaceae
f__Prevotellaceae
f__Fusobacteriaceae
p__Fusobacteria
g__Fusobacterium
c__Fusobacteriia
o__Fusobacteriales
LDA SCORE (log 10)
D
Acetic acid
Propionic acid
Butyric acid
Isobutyric acid
Isovaleric acid
Hexanoic acid
Metabolite concentration (ng/mg)
EP
EF

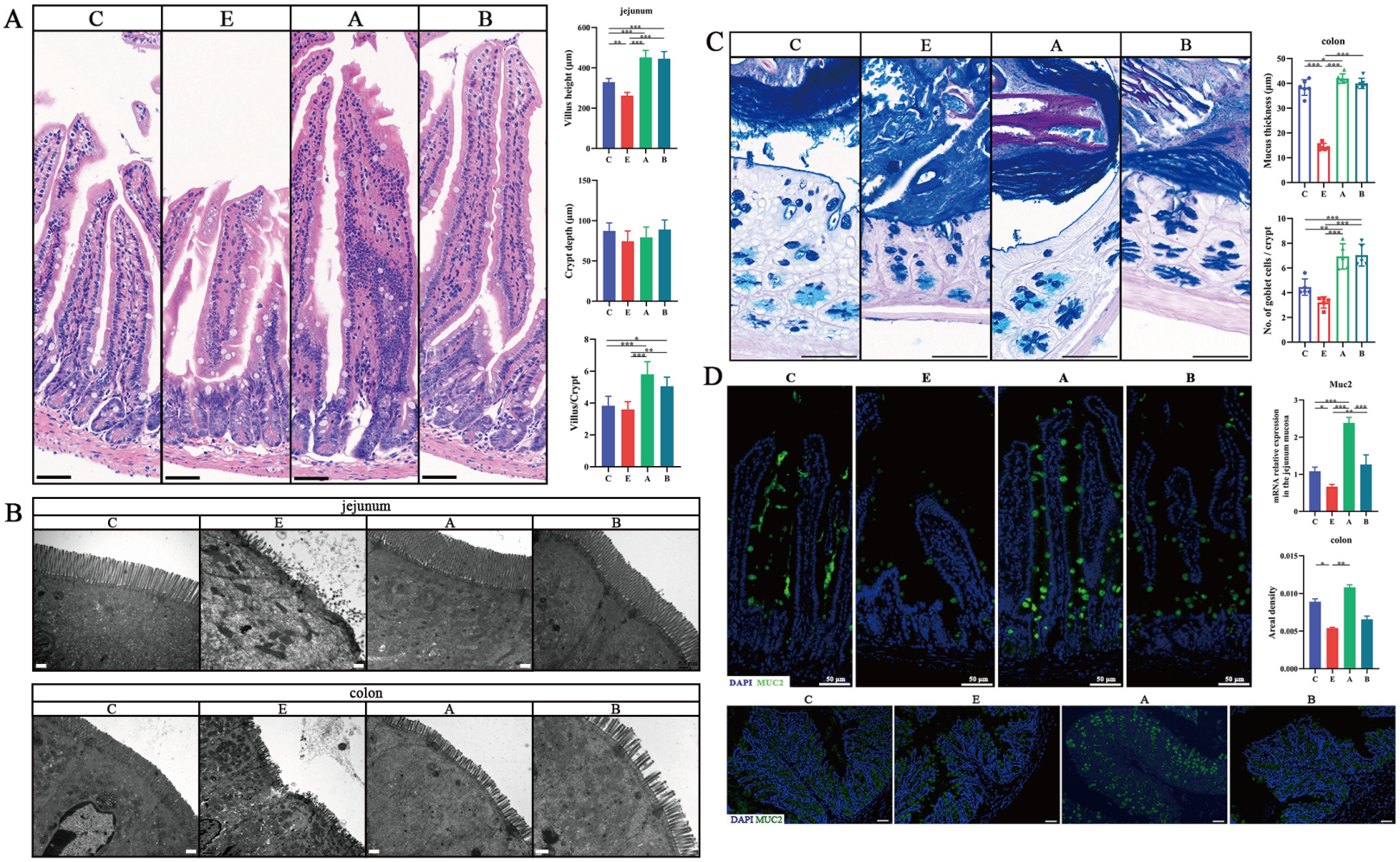
A
C
E
A
B
jejunum
Villus height (μm)
Crypt depth (μm)
Villus/Crypt
B
jejunum
colon
C
D
colon
Mucus thickness (μm)
No. of goblet cells / crypt
Muc2
mRNA relative expression in the jejunum mucosa
Areal density
DAPI MUC2
50 μm

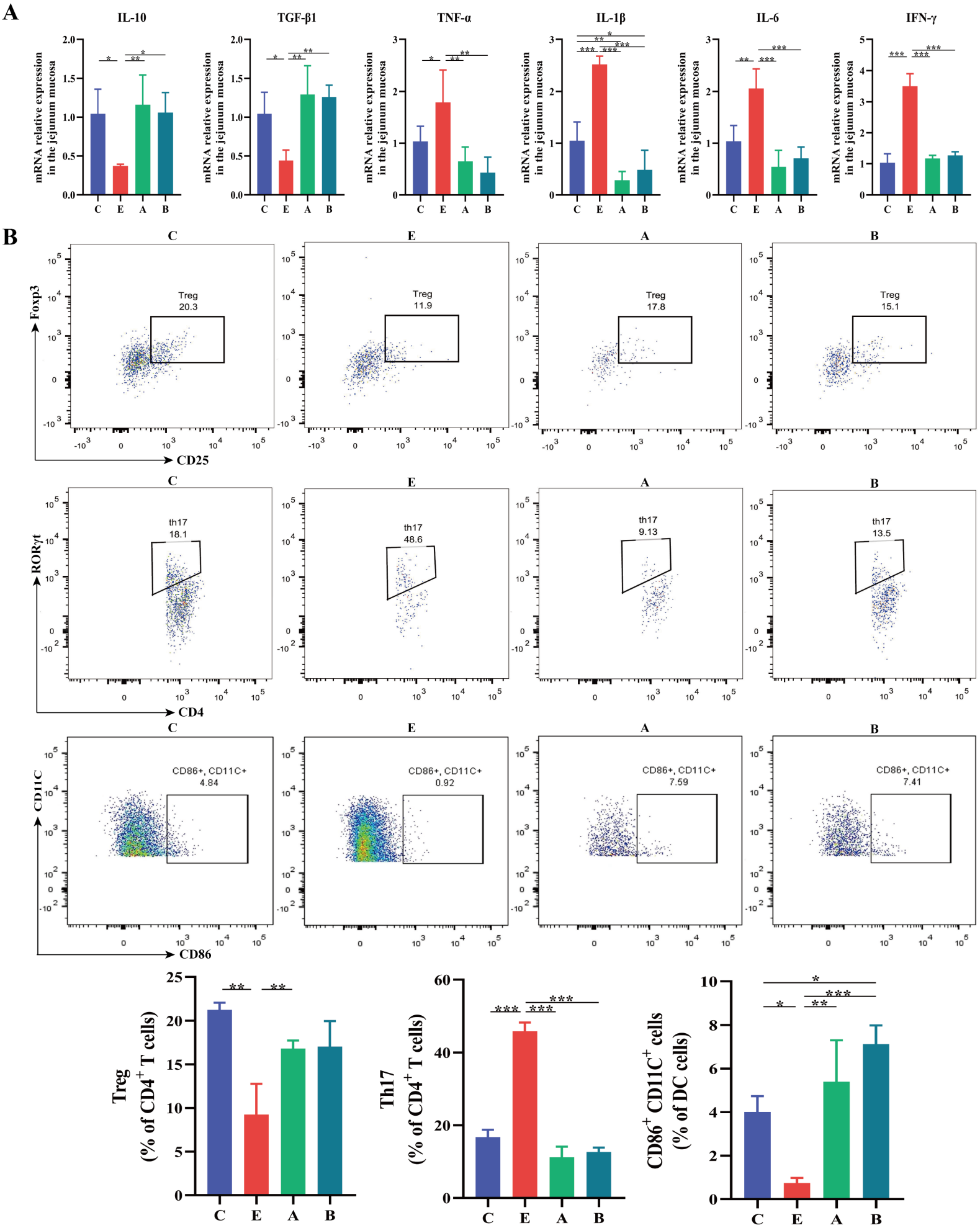
A
IL-10
TGF-β1
TNF-α
IL-1β
IL-6
IFN-γ
mRNA relative expression in the jejunum mucosa
C E A B
B
Foxp3
CD25
Treg 20.3
Treg 11.9
Treg 17.8
Treg 15.1
RORγt
CD4
th17 18.1
th17 48.6
th17 9.13
th17 13.5
CD11C
CD86
CD86+, CD11C+ 4.84
CD86+, CD11C+ 0.92
CD86+, CD11C+ 7.59
CD86+, CD11C+ 7.41
Treg (% of CD4+ T cells)
Th17 (% of CD4+ T cells)
CD86+ CD11C+ cells (% of DC cells)

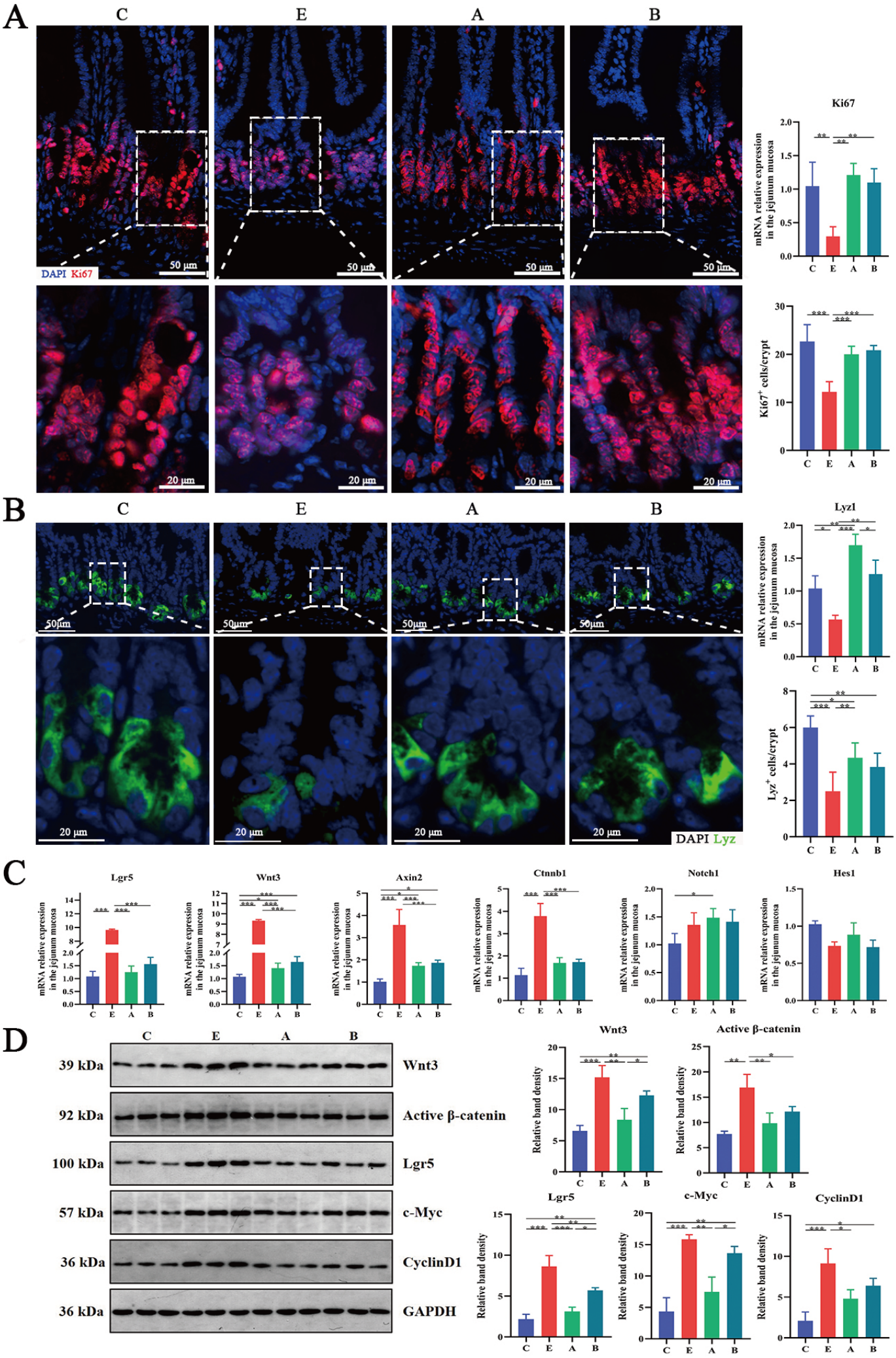
A
C
E
A
B
DAPI Ki67
50 μm
20 μm
Ki67
mRNA relative expression in the jejunum mucosa
Ki67+ cells/crypt
B
Lyz1
Lyz+ cells/crypt
DAPI Lyz
C
Lgr5
Wnt3
Axin2
Ctnnb1
Notch1
Hes1
mRNA relative expression in the jejunum mucosa
D
39 kDa
Wnt3
92 kDa
Active β-catenin
100 kDa
Lgr5
57 kDa
c-Myc
36 kDa
CyclinD1
36 kDa
GAPDH
Relative band density

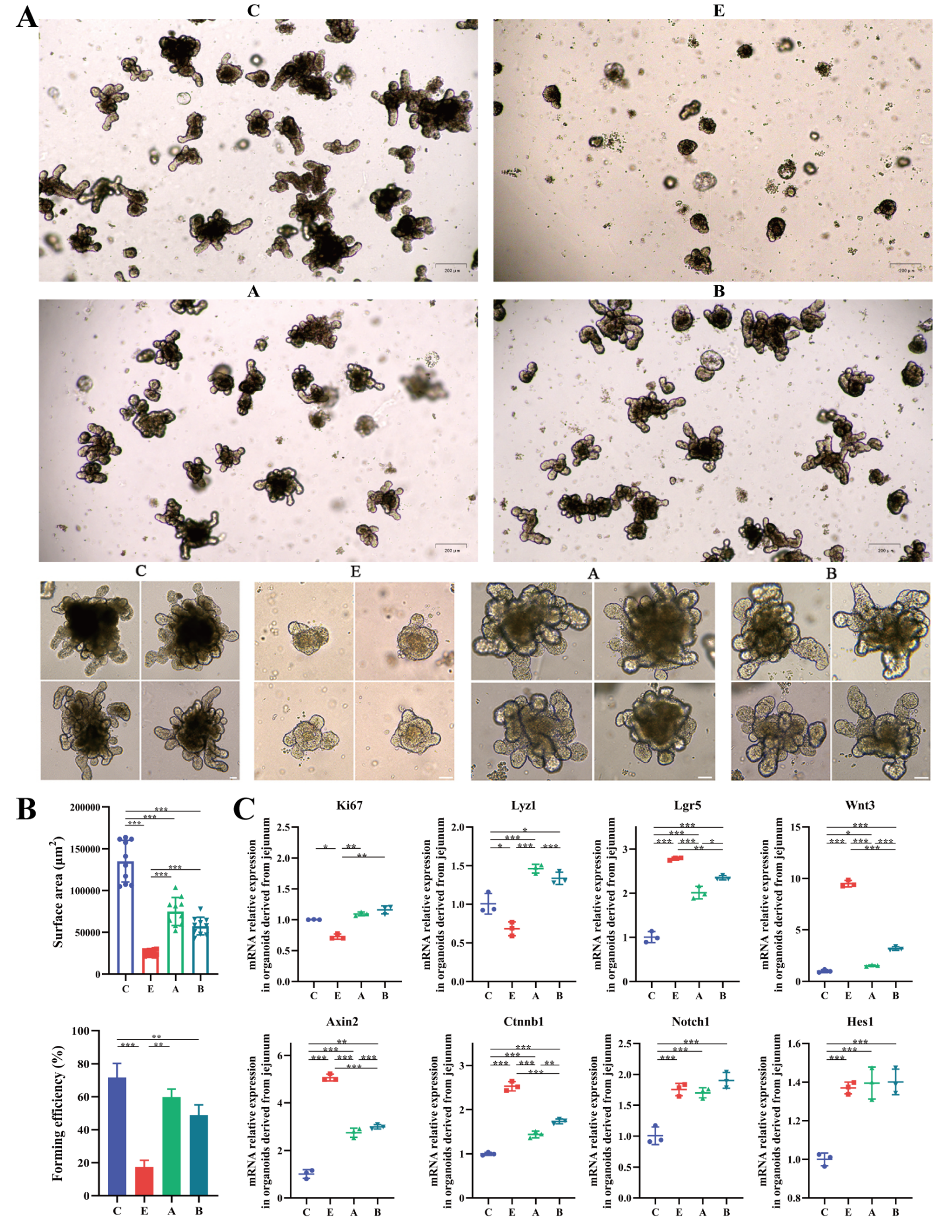
A
C
E
A
B
C
E
A
B
B
Surface area (μm²)
Forming efficiency (%)
C
Ki67
Lyz1
Lgr5
Wnt3
Axin2
Ctnnb1
Notch1
Hes1
mRNA relative expression in organoids derived from jejunum

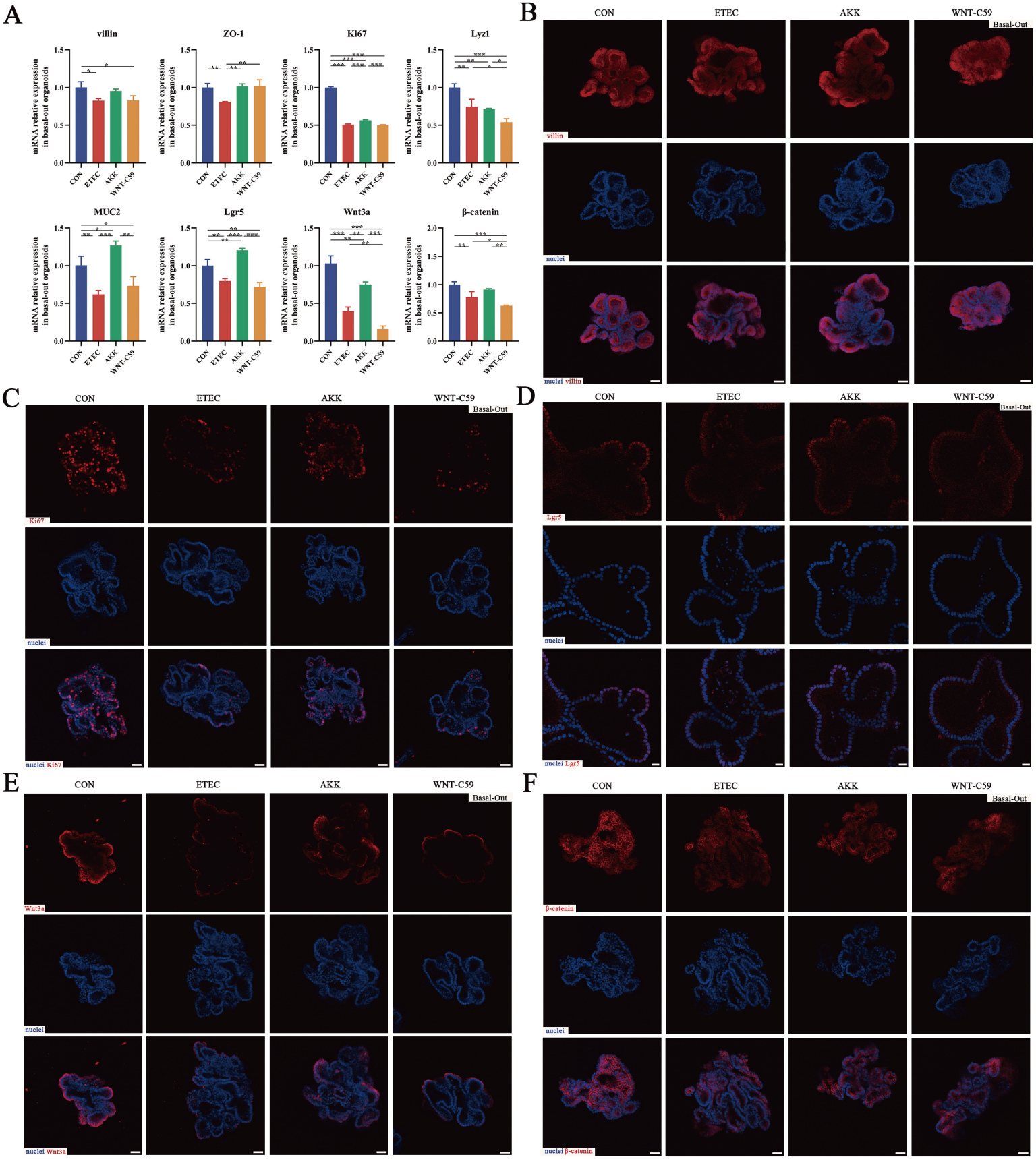
A
villin
ZO-1
Ki67
Lyz1
MUC2
Lgr5
Wnt3a
β-catenin
mRNA relative expression in basal-out organoids
CON
ETEC
AKK
WNT-C59
B
CON
ETEC
AKK
WNT-C59
Basal-Out
villin
nuclei
nuclei villin
C
Ki67
nuclei
nuclei Ki67
D
Lgr5
nuclei
nuclei Lgr5
E
Wnt3a
nuclei
nuclei Wnt3a
F
β-catenin
nuclei
nuclei β-catenin

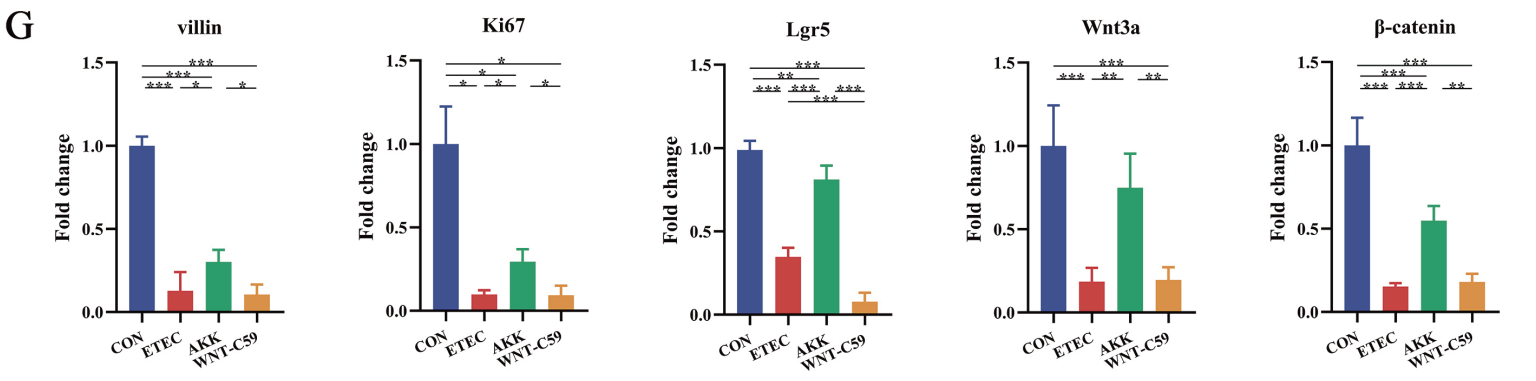
G
villin
Ki67
Lgr5
Wnt3a
β-catenin
Fold change
CON
ETEC
AKK
WNT-C59

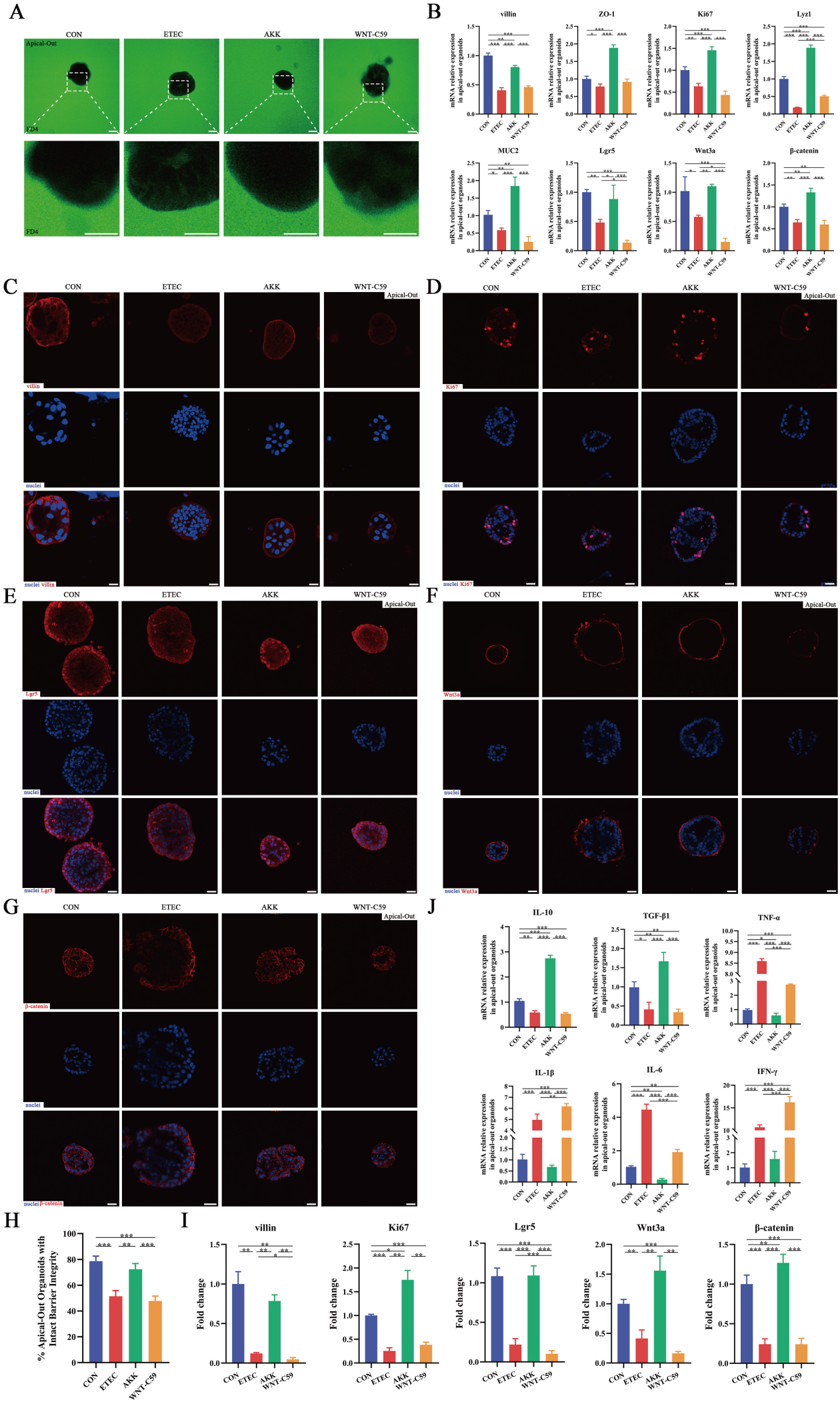
A
CON
ETEC
AKK
WNT-C59
Apical-Out
FD4
B
villin
ZO-1
Ki67
Lyz1
MUC2
Lgr5
Wnt3a
β-catenin
mRNA relative expression in apical-out organoids
C
villin
nuclei
D
Ki67
E
Lgr5
F
Wnt3a
G
β-catenin
J
IL-10
TGF-β1
TNF-α
IL-1β
IL-6
IFN-γ
H
% Apical-Out Organoids with Intact Barrier Integrity
I
Fold change